SYNTHESIS AND CHARACTERIZATION OF MODIFIED SBA-15 FOR CO_2 REFORMING OF CH_4

(SINTESIS DAN PERINCIAN BAGI UBAHSUAI SBA-15 UNTUK CO_2 PEMBAHARUAN CH_4)

HERMA DINA BINTI SETIABUDI
NURUL AINI BINTI MOHAMED RAZALI
MIOR AHMAD KHUSHAIRI BIN MOHD ZAHARI
SYAMSUL BAHARI BIN ABDULLAH

RESEARCH VOTE NO:
RDU140398

Faculty of Chemical & Natural Resources Engineering
Universiti Malaysia Pahang

2017

ACKNOWLEDGEMENT

I would like to acknowledge Universiti Malaysia Pahang for funding this research activity through RDU140398 and Chemical Engineering Laboratory, FKKSA UMP for equipment and facilities available. I also would like to extend my gratitude to team members who always help and gave advice during this research period. Thank you to my students that works out the research plan accordingly. Last but not least, to my dearest family.

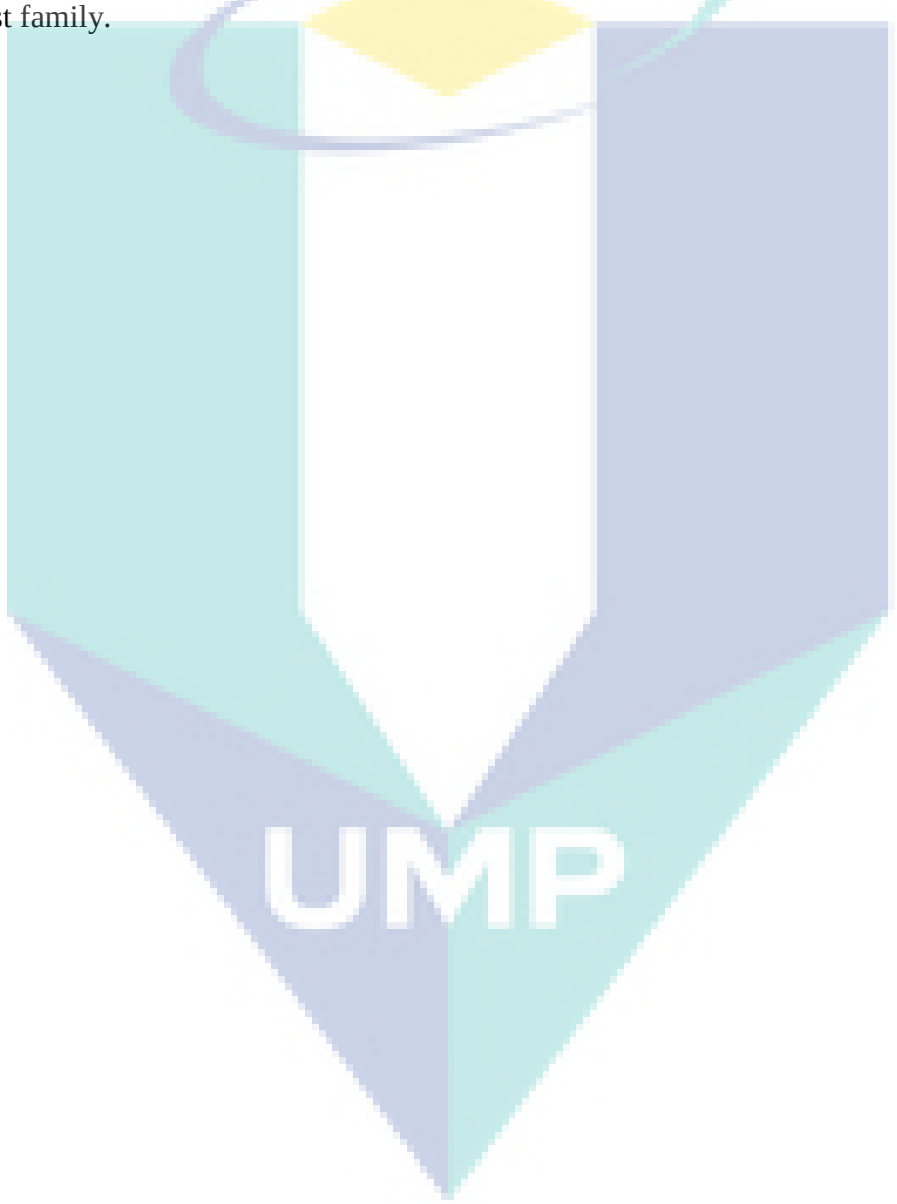

ABSTRACT

SYNTHESIS AND CHARACTERIZATION OF MODIFIED SBA-15 FOR CO_2 REFORMING OF CH_4

(Keywords: Ni/SBA-15, CH_4 reforming; TEOS/P123, Ni loading, Ni-loading method)

CO_2 reforming of CH_4 has been studied extensively using variety of metal supported catalyst, including Ni/SBA-15. However, during lengthy stability testing, Ni/SBA-15 is gradually deactivated because of carbon deposition. Owing to the fact that the preparation of well dispersed Ni/SBA-15 is desired to inhibit carbon formation, thus the effects of TEOS/P123 mass ratio (1.5, 2.21 and 3.0), amount of Ni loading (3, 5 and 10 wt%) and Ni-loading method (impregnation (IM), ion exchange (IE) and physical mixing (PM)) on the properties and catalytic activity of Ni/SBA-15 were studied. The catalysts were characterized using XRD, BET, SEM, TEM, H_2-TPR and TGA, while the catalytic activities were carried out using microcatalytic reactor. For the effect of TEOS/P123 ratio, the result clearly indicated that TEOS/P123 mass ratio of 2.21 was the optimal synthesis ratio of Ni/SBA-15 which produces the well-ordered hexagonal mesoporous structure with the highest Ni-support interaction, Ni–O–Si. The catalytically favorable textural properties of Ni/SBA-15(R2.21) enhanced the dispersion of metal particles, improved the catalyst activity, increased the catalyst stability and reduced the carbon deposition. For the effect of Ni loading, the result showed that the maximum formation of Ni–O–Si were achieved at 5 wt%, while further increased in Ni loading stimulate the agglomeration of Ni particles. The presence of Ni–O–Si in 5Ni/SBA-15 enhanced the stabilization of the active Ni species on SBA-15 support, minimized the growth of encapsulating graphite carbon and thus enhanced the activity and stability of catalyst. For the effect of Ni-loading method, the result showed that the Ni/SBA-15(IE) has higher formation of Ni–O–Si, which altered the properties of catalyst towards an excellent catalytic performance. This study successfully prepared well dispersed Ni/SBA-15 using IE method with TEOS/P123 of 2.21 and 5 wt% Ni loading.

Key researchers: Herma Dina Binti Setiabudi, Nurul Aini Binti Mohamed Razali, Mior Ahmad Khushairi Bin Mohd Zahari, Syamsul Bahari Bin Abdullah

E-mail : herma@ump.edu.my; Tel. No. : 09-5492836; Vote No. : RDU140398

ABSTRAK

SINTESIS DAN PERINCIAN BAGI UBAHSUAI SBA-15 UNTUK CO_2 PEMBAHARUAN CH_4

(Kata Kunci: Ni/SBA-15, pembaharuan CH_4; TEOS/P123, beban Ni, kaedah Ni)

CO_2 pembaharuan CH_4 telah dikaji secara meluas menggunakan pelbagai logam disokong pemangkin, termasuk Ni/SBA-15. Walau bagiamanapun, semasa ujian kestabilan yang panjang, Ni/SBA-15 dinyahaktifkan secara beransur-ansur kerana pemendapan karbon. Disebabkan hakikat bahawa penyediaan bagi Ni/SBA-15 yang baik adalah dikehendaki untuk menhalang pembentukan karbon, oleh tiu kesan nisbah jisim TEOS/P123 (1.5, 2.21 dan 3.0), jumlah beban Ni (3,5 dan 10 wt%) dan kaedah memasukan Ni (pengisitepuan (IM), pertukaran ion (IE) dan pencampuran fizikal (PM)) kepada sifat-sifat dah aktiviti pemangkin Ni/SBA-15 telah dikaji. Pemangkin dicirikan dengan menggunakan XRD, BET, SEM, TEM, H_2-TPR dan TGA, manakala aktiviti pemangkin telah dijalankan dengan menggunkan reactor mikrokatalitik. Untuk kesan nisbah TEOS/P123, keputusan jelas menunjukan bahawa 2.21 nisbah jisim TEOS/P123 adalah nisbah sistesis oprimum NI/SBA-15 yang menghasilkan structur mesostruktur heksagon yang teratur dengan interaksi Ni sokongan, Ni–O–Si yang paling tinggi. Ciri-ciri tekstur katalitik Ni/SBA-15(R2.21) meningkatkan penyebaran zarah logam, membaiki aktiviti pemagkin, meningkatkan ketabilan pemangkin dan mengurangkan pemendapan karbon. Untuk kesan beban Ni, hasil kajian menunjukan bahawa pembentukan maksimum Ni–O–Si dicapai pada 5wt%, sementara peningkatan yang berterusan pada jumlah beban Ni merangsang aglomerasi zarah Ni. Kehadiran Ni–O–Si dalam 5Ni/SBA-15 mempertingkatkan pentabilan species Ni aktif pada SBA-15 sokongan, mengurangkan pertumbuhan himpunan grafit karbon dan dengan itu meningkatkan aktiviti dan kestabilan pemagkin. Untuk kesan kaedah Ni-loading, hasilnya menunukan bahawa Ni/SBA-15(IE) mempunyai pembentukan Ni–O–Si yang lebih tinggi, yang mengubah sifat-sifat pemangkin kea rah prestasi pemangkin yang sangta baik. Kajian ini berjaya menyediakan Ni/SBa-15 yang baik dengan menggunakan kaedah IE dengan TEOS/P123=2.21 dan 5wt% beban Ni.

Penyelidik utama: Herma Dina Binti Setiabudi, Nurul Aini Binti Mohamed Razali, Mior Ahmad Khushairi Bin Mohd Zahari, Syamsul Bahari Bin Abdullah

E-mail : herma@ump.edu.my; Tel. No. : 09-5492836; Vote No. : RDU140398

TABLE OF CONTENTS

LIST OF TABLES

Table No. **Title** **Page**

LIST OF FIGURES

Figure No. **Title** **Page**

LIST OF SYMBOLS

%	Percentage
wt%	Weight percentage
ml	millilitre
θ	Angle
X_{CO2}	Conversion of carbon dioxide
X_{CH4}	Conversion of methane
F	Molar flow rate
P	Partial pressure
Ps	Saturated pressure
A	Area
m	Mass
λ	Wavelength of ray
˚C	Degrees Celsius
kg	kilogram
g	gram
h	hour
mL	mililiter
min	minute

LIST OF ABBREVIATIONS

Al_2O_3	Aluminium oxide
BET	Breneuer-Emmett Teller
CH_4	Methane
CO	Carbon monoxide
Co	Cobalt
CO_2	Carbon dioxide
FTIR	Fourier-transform infrared spectroscopy
H_2	Hydrogen
H_2O	Water
H_2SO_4	Sulphuric acid
MCM-41	Mobil Catalytic Material Number 41
N_2	Nitrogen
N_2O	Nitrous Oxide
Na	Sodium
Na_2O_3	Sodium dioxide
Ni	Nickel
NiO	Nickel oxide
O_3	Ozone
P123	Pluronic triblock copolymer
Pt	Platinum
Rh	Rhodium
Ru	Ruthenium
SBA-15	Santa-Barbara Amorphous 15
SiO_2	Silicon dioxide
TEM	Transmission electron microscope
XRD	X-Ray diffraction

CHAPTER 1

INTRODUCTION

1.1 BACKGROUND OF THE STUDY

In recent years, climax change has become a serious world-wide environmental problem and the negative effects of greenhouse gas emission on people's health are unavoidable fact. As CO_2 is one of the main contributors to the greenhouse effect and hence causes climate change, the elimination of CO_2 has been an attracting interest from the environmental perspective. The CO_2 reforming of CH_4 (so-called dry reforming) is one of the CO_2 elimination methods and has recently attracted considerable attention (Ababou et al., 2015; Abderrahim et al., 2011; Sidik et al, 2016), due to the simultaneous utilization and reduction of two greenhouse gases, CO_2 and CH_4, into synthesis gas (syngas). The syngas produced has a lower H_2/CO ratio than those available in industrial processes, which is preferred for the synthesis of valuable oxygenated chemicals and long-chain hydrocarbons.

The CO_2 reforming of CH_4 has been studied extensively using variety of supported metal catalysts including transition metal-based catalysts (Ni, Co, Cu, Fe) (Donphai et al., 2014; Sajjadi et al., 2013; Theofanidis et al., 2015; Zhang et al., 2014) and noble metal-based catalysts (Rh, Ru, Pd, Pt, Ir) (Richardson et al., 2003; Tao et al., 2010; Xu et al., 2016). It has been reported that noble metal-based catalysts especially Rh based ones have the higher stability and resistance against coke deposition (Nematollahi et al., 2011). However, restricted availability and high cost limited their use in industrial level. Therefore, the substitution of noble metals by transition ones, especially Ni (Khajenoori et al., 2015; Sidik et al., 2016) is nowadays attractive owing to its wider availability, lower cost and better catalytic performance (Liu et al., 2009; Qi et al., 2015).

Several materials have been used as supports for Ni-based catalysts including metal oxides (Al-Fatesh et al., 2011; Benguerba et al., 2015; Dan et al., 2012), zeolites (Bacariza et al., 2016) and siliceous materials (Berndt et al., 2016; Sidik et al., 2016). In 1998, Zhao et al. (1998) successfully synthesized mesoporous silica SBA-15 (Santa Barbara Amorphous) under acidic condition using a nonionic surfactant (Pluronic 123, P123) as template and tetraethyl orthosilicate (TEOS) as silica source. SBA-15 has attracted great attention in catalysis field owing to its high surface areas (600 – 1000 m^2/g), hexagonal arrays of uniform tubular channels with tunable pore diameters (5 – 30 nm) and high thermal stability due to the thicker pore walls (3 – 6 nm) (Abdullah et al., 2010). Moreover, the abundant surface silanol groups and mesostructured properties make SBA-15 as a good candidate for immobilizing transition metal precursors inside the pores of the support (Charan & Rao, 2015).

It has been reported that during lengthy stability testing of Ni/SBA-15 towards CO_2 reforming of CH_4, Ni/SBA-15 is gradually deactivated because of carbon deposition (Natesakhawat et al., 2005). Several methods have been used to reduce carbon deposition on Ni/SBA-15 by preparing highly dispersed Ni/SBA-15 catalyst including modification of the support, addition of alkaline metal and addition of co-promoter. Ahmad and Hossain (2015) reported that the methodologies of support preparation greatly influence the morphology structure of support and thus affecting the dispersion of metal particles on the support. Whereas, Setiabudi et al. (2012) and Sidik et al. (2016) found that the amount of metal content and method of metal loading affected the interaction of metal with the support, which further affecting the dispersion of metal particles on the catalyst support. Owing to the fact that the preparation of well dispersed Ni/SBA-15 is desired to inhibit coke formation, thus several effects were studied to improve the properties and catalytic activity of Ni/SBA-15 towards CO_2 reforming of CH_4.

1.2 OBJECTIVES

The objectives of this research are as follows:

1. To synthesize and characterize Ni/SBA-15 catalysts
2. To study the effect of TEOS/P123 mass ratio on the properties and catalytic activity of Ni/SBA-15 towards CO_2 reforming of CH_4.

3. To study the effect of Ni loading on the properties and catalytic activity of Ni/SBA-15 towards CO_2 reforming of CH_4.
4. To study the effect of Ni-loading methods on the properties and catalytic activity of Ni/SBA-15 towards CO_2 reforming of CH_4.

1.3 SCOPES OF STUDY

The scopes of this research as follows:

i) Preparation and Characterization of Ni/SBA-15 catalysts

SBA-15 was synthesized from tetraethyl orthosilicate precursor (TEOS) and Pluronic P123 triblock-copolymer (P123). Ni/SBA-15 was prepared by impregnation method of SBA-15 and Ni salt precursor, Nickel (II) Nitrate hexahydrate, $Ni(NO_3)_2.6H_2O$. Several Ni/SBA-15 catalysts were prepared by varying the mass ratio of TEOS/P123, amount of Ni loading and Ni-loading methods. The synthesized catalysts were characterized using X-ray Diffraction (XRD), surface area analyser (BET), Fourier-Transform Infrared Spectroscopy (FTIR), Thermogravimetric Analysis (TGA), Transmission Electron Microscopy (TEM), Scanning Electron Microscope (SEM) and H_2-TPR analyser.

ii) Study on the effect of TEOS/P123 mass ratio on the properties and catalytic activity of Ni/SBA-15 towards CO_2 reforming of CH_4

The effect of TEOS/P123 mass ratio on the properties and catalytic activity of Ni/SBA-15 towards CO_2 reforming of CH_4 were studied by varying the mass ratio of TEOS/P123 (1.5, 2.21, 3.0 and 3.5). The properties of catalysts were analyzed using XRD, BET, FTIR, SEM, TEM and TGA. The catalytic activity of catalysts was carried out in a microcatalytic quartz reactor at 800 ˚C and atmospheric pressure using $CO_2/CH_4/N_2$ with a feed ratio of 1/1/1.

iii) Study on the effect of Ni loading on the properties and catalytic activity of Ni/SBA-15 towards CO_2 reforming of CH_4

The effect of Ni loading on the properties and catalytic activity of Ni/SBA-15 towards CO_2 reforming of CH_4 were studied by varying the amount of Ni (3, 5 and 10 wt%). The properties of catalysts were analyzed using XRD, BET, FTIR,

TEM, TGA and H_2-TP. The catalytic activity of catalysts was carried out in a microcatalytic quartz reactor at 800 ˚C and atmospheric pressure using $CO_2/CH_4/N_2$ with a feed ratio of 1/1/1.

iv) Study on the effect of Ni-loading methods on the properties and catalytic activity of Ni/SBA-15 towards CO_2 reforming of CH_4

The effect of Ni-loading methods on the properties and catalytic activity of Ni/SBA-15 towards CO_2 reforming of CH_4 were studied by varying the preparation methods of Ni loading (impregnation (IM), ion exchange (IE) and physical mixing (PM)). The properties of catalysts were analyzed using XRD, BET, SEM, FTIR and TGA. The catalytic activity of catalysts was carried out in a microcatalytic quartz reactor at 800 ˚C and atmospheric pressure using $CO_2/CH_4/N_2$ with a feed ratio of 1/1/1.

CHAPTER 2

LITERATURE REVIEW

2.1 CO_2 EMISSION AND GLOBAL WARMING

Carbon dioxide (CO_2) is naturally present in the atmosphere as part of the Earth's carbon cycle that is the natural circulation of carbon among the atmosphere, oceans, soil, plants, and animals. Human activities are altering the carbon cycle, both by adding more CO_2 to the atmosphere and by influencing the ability of natural sinks, like forests, to remove CO_2 from the atmosphere (Mustapa & Bekhet, 2015). For the last few decades, energy consumption in Malaysia has increased and thus increases the amount of CO_2 emissions (Lee et al., 2013). CO_2 emissions in Malaysia were recorded to have an annual increase rate of 4.6% for the year 1971 to 2012 (Begum et al., 2015). The major source of CO_2 emission is caused by transportation activities which contribute up to 97.1% from the total emission (Lee et al., 2013). Transportation activities include the emission from the motor vehicles both individually owned vehicles as well as businesses owned vehicles. There are over 19 million registered vehicles in the country. This high number of vehicles in Malaysia has caused the high emission of carbon dioxide. Other than that, industries also contribute to the CO_2 emission in Malaysia (Azlina et al., 2014). The emission of CO_2 from all sectors in Malaysia have reached 279 million metric tonnes while the emission per capita for all sectors were recorded as 10.7 metric tonnes in 2007 (Mugable, 2013). CO_2 also emitted from power stations such as fossil fuel-fired power plants. Fossil fuel-fired power plants use natural gas, petroleum, coal or any form of solid, liquid, or gaseous fuel derived from such material for the purpose of generating electricity (Begum et al., 2015).

Other than Malaysia, the global CO_2 emissions also increase from year to year due to the high consumption of fossil fuel. World CO_2 emissions from the consumption

of fossil fuels are expected to grow at an average rate of 2.1% per year from 2003 to 2030 (Sina et al., 2015). The world CO_2 emission from the consumption of fossil fuels is predicted to increase from about 25,000 billion metric tons in 2003, to more than 40,000 billion metric tons by 2030 (Jibran et al. , 2015). CO_2 gas is primary greenhouse gases and the most important anthropogenic greenhouse gases. CO_2 gas can negatively effects the environment, human health and plants. The most significant effect of CO_2 gas is global warming and greenhouse effect (Guerrero et al., 2005). When energy arrives from the sun in the form of visible light and ultraviolet radiation, most of the light energy from the sun is emitted in wavelengths shorter than 4,000 nanometer. Some of the received energy is emitted as infrared radiation and left the Earth (Lee & Holder, 2001). The heat energy released from the earth is released in wavelengths longer than 4,000 nanometer. CO_2 gas does not absorb the energy from the sun, but it does absorb some of the heat energy released from the earth. This means CO_2 lets the light energy in, but does not let all of the heat energy out (Lee et al., 2013). When a molecule of CO_2 absorbs heat energy, it goes into an excited unstable state. It can become stable again by releasing the energy it absorbed. Some of the released energy will go back to the earth and some will go out into space (Lee & Holder, 2001). The net effect is that most of the outgoing radiation is kept within the atmosphere instead of escaping into space. Thus the temperature in the Earth keeps increasing and global warming occur (Lee et al., 2013). The Intergovernmental Panel on Climate Change reported that eleven of the twelve years from 1995 to 2006 rank among the 12 warmest years in the instrumental record of global surface temperature since 1850. The total temperature increase from 2001 to 2005 is about 0.76 °C. It is predicted a rise in the average global surface temperature of about 2 °C between 1990 and 2100 (Dijkstra & Morgan, 2012).

Global warming also brings a lot of negative effects. The first one is the melting of the glacier and ice (Ahmad & Hossain, 2015). Glaciers all over the world have been melting for at least the last 50 years, and the rate of melting is speeding up as the temperature of the earth keep increasing. The polar ice cap is melting at the alarming rate of nine percent per decade (Zhang & Li, 2015). Arctic ice thickness has decreased 40 percent since the 1960s (Ahmad & Hossain, 2015). Arctic sea ice extent set an all-time record low in September 2007, with almost half a million square miles less ice than the previous record set in September 2005. Over the past 3 decades, more than a million square miles of perennial sea ice has disappeared (Kowalski et al., 2015). The rapid

melting of the glacier has caused the animal like polar bear and penguins to face extinction as they lost their habitats (Thoma et al., 2015). The numbers of Adelie penguins have fallen from 32,000 breeding pairs to 11,000 in 30 years because of the melting of glacier (Jennifer et al., 2013). Other than that, global warming will also cause the sea level to rise. There are two major mechanisms that caused the sea level to rise. First, shrinking land ice, such as mountain glaciers and polar ice sheets, is releasing water into the oceans. Second, as ocean temperatures rise, the warmer water expands (Lovell, 2015). Trapped within a basin bounded by the continents, the water has nowhere to go but up. In some parts of the world, especially low-lying river deltas, local land is sinking making sea levels that much higher (Valle et al., 2014). Sea-level rise will affect the worldwide proliferation of humans and their preferences for living in and developing coastal areas. Sea level rise significantly threaten the safety of the people who live on or within 50 miles of the coast (Isobe, 2013). Other than that, rising seas will increase coastal erosion, pollution, storm damage, and flooding. Rising of sea level will also pose threats to coastal roads, bridges, jetties, breakwaters, docks, piers, and waterfront property (Crank & Jacobe, 2015). Intruding salt water might contaminate groundwater supplies and threaten landfill and hazardous-waste sites (Allison et al., 2015).

Apart from these, global warming will also affect evapotranspiration that is the movement of water into the atmosphere from land and water surfaces and plants due to evaporation and transpiration (Devoy, 2015). This will in turn increase the drought in dry areas where the increased evaporation is not compensated for by more precipitation. In drier regions, evapotranspiration may produce periods of drought and cause below-normal levels of rivers, lakes, groundwater, and lack of enough soil moisture in agricultural areas (Cui & Kump, 2015). Precipitation has declined in the tropics and subtropics since 1970 (Molloy & Mihaltcheva, 2013). Southern Africa, the Sahel region of Africa, southern Asia, the Mediterranean, and the U.S. Southwest are getting drier. This affects the life of the people in the dry places as they do not have enough water supplies (Habib et al., 2013). Besides, global warming will also cause extreme weather to happen. Global warming is making hot days hotter, rainfall and flooding heavier, hurricanes stronger and droughts more severe (Roscher et al., 2011). This intensification of weather and climate extremes will be the most visible impact of global warming in everyday lives. It is also causing dangerous changes to the landscape of our world,

adding stress to wildlife species and their habitat (Devoy, 2015). Therefore it is critical to find a way to decrease the concentration of CO_2 gas in the atmosphere in order to decrease global warming.

2.2 ALTERNATIVES TO REDUCE CO_2 IN THE ATMOSPHERE

2.2.1 Monoethanolamine (MEA) scrubbing

From previous study carried out by Jung et al., (2013), CO_2 capture process using aqueous Monoethanolamine (MEA) is one of the important alternative for reducing CO_2 emission to the atmosphere (Jung et al., 2013). The MEA process primarily consists of an absorber, a heat exchanger and a stripper (Moioli et al., 2012)The CO_2 in flue gas enters to the bottom of the absorber and the MEA solvent enters to the top of the absorber. The MEA solvent selectively absorbs the CO_2 via exothermic reaction (Moioli et al., 2012). The MEA process has been considered as the most effective technique for post-combustion CO_2 capture due to its high reactivity for even low CO_2 concentration flue gas (Alie et al., 2005). However, MEA process consumes a lot of heat energy for solvent regeneration because the MEA solvent is aqueous based. The reboiler heat energy occupies about 80% of the entire energy consumption for CO_2 capture process. The high energy consumption for the process makes the cost to be high and this limits its application (Singh et al., 2003)

2.2.2 Lime-soda process

Lime-soda process is one of the negative emission technology used to decrease the concentration of CO_2 in the atmosphere (Keith & Wong, 2006). Negative emissions technology is a technology which employs an 'industrial' process of some kind to achieve the absorption of the CO_2 gas. Function of soda-lime process is to generate a concentrated CO_2 stream from the very dilute CO_2 in the air (Cebrucean et al., 2014). In a lime-soda process, alkali absorbent such as aqueous sodium hydroxide is brought into contact with the atmosphere using a conventional scrubbing tower arrangement. Aqueous sodium hydroxide will adsorb the CO_2 gas in the atmosphere and sodium carbonate solution is formed. The resulting sodium carbonate solution is then regenerated by reaction with lime (calcium oxide) (Karimi et al., 2011). There are a few

drawbacks in this technology. Firstly, the energy requirements for this technology are significant. Cost to carry out this process will be high due to the high energy requirement. The capital equipment price for lime-soda process is very high. The total cost of generating 0.1 ppm change in atmospheric CO_2 concentrations per annum would be US$ 120 Billion which is very high (Keith & Wong, 2006).

2.2.3 Augmented Ocean Disposal

Augmented ocean disposal is a technique that uses the lime in ocean to trap CO_2 in a stable mineral form. Lime is generated using lime kilns and is then transported to mid-ocean using ships (Kruger, 2010). The lime is hydrated and then released into the surface layers of the ocean where it reacts with CO_2 dissolved in the water. This has the effect of lowering the pH of the surface waters, which in turn leads to the rapid absorption of an equivalent quantity of CO_2 from the atmosphere (Kajishima et al., 1997). In this technique, the cost is not very high because it does not involve complicated equipment and only lime is used. Thus, this technology becomes potentially cost effective. However, the drawback of this technology is the risk to the environment caused by such a major intervention into the natural balance of the ocean ecosystem (Kruger, 2010). The pH of the sea water will be lower during the process and this will a great threat to the marine life. This is because most of the marine life is very sensitive to the change in the pH of the water. So, augmented ocean disposal method is not a good alternative as it will disturb the ecosystem (McGlashan et al., 2012)).

2.2.4 Biochar Process

Biochar process is a process that involves the production of enriched carbon bio-material by partially combusting biomass in a low oxygen environment in a process called slow pyrolysis (Huang et al., 2015). In this process, the carbon that is previously absorbed from the atmosphere is fixed effectively because the biomass fixes CO_2 from the atmosphere as stable, solid carbon in the biochar. The char produced can be land filled or used as fertiliser (Rebitanim et al., 2013). The advantages of biochar process are it avoid the emission of CO_2 gas from substitution of syngas for fossil fuel, it can reduce the CO_2 emission from agriculture field due to the reduction in the fertiliser usage (Wu et al., 2015). However, there are also a few drawbacks for biochar process.

First, the cost for the biochar process is very high. Other than that, the effect of biochar process toward the reduction of the CO_2 concentration in the atmosphere is not significant although the CO_2 gas can be fixed effectively (Thomazini et al., 2015). From the study by Zhang et al. (2014), even if the 2.6 Billion portion of the world population who use traditional biomass were to be issued with biochar process, the ppm impact would be limited at between 0.15 to 0.015 ppm per annum only (Zhang et al., 2014). So biochar process is not a good alternative to reduce the CO_2 concentration in the atmosphere.

2.2.5 CO_2 Reforming

CO_2 reforming is a method of producing synthesis gas (mixtures of hydrogen and carbon monoxide) from the reaction of carbon dioxide with hydrocarbons such as methane. This process is also known as dry reforming reaction which is an important catalytic process (Li et al., 2015). The chemical equation for CO_2 reforming is as follow.

$$CO_2 + CH_4 \rightarrow 2\ H_2 + 2\ CO \qquad (2.1)$$

CO_2 reforming is a reversible exothermic reaction. 247.0 kJ/mol of energy is given off from this reaction. The CO_2 reforming reaction is also thermodynamically favourable with ΔG_{298K} = – 130.8 kJ/mol (He et al., 2015)It is a clean and environmental friendly technology as two of the major greenhouse gases that are CO_2 and methane can be eliminated from atmosphere. Methane gas is a more potent greenhouse gases than CO_2 and it is approximately 200 times more than CO_2 in atmosphere (Kaydouh et al., 2015). Other than that, methane gas is the second most prevalent greenhouse gases emitted from human activities. Methane gas is much more effective than carbon dioxide at trapping heat in the atmosphere. Methane is much more complicated once it gets into the atmosphere because it reacts with a lot of different important chemicals. Methane in the atmosphere also creates ground-level ozone. And ozone isn't only bad for human health; it also contributes to global warming (Liu et al., 2015). Both CO_2 and methane gas should be eliminated from atmosphere in order to reduce the impact of climate change and global warming effectively. CO_2 reforming reaction becomes a promising alternative to reduce both greenhouse gases in

atmosphere (Liu et al., 2014). Apart from these, the major product from this reaction is hydrogen gas, H2 which is a useful chemical block and hydrogen gas can be used to produce hydrochloric acid, methanol and even used in a fuel cell. In industry, hydrogen is used mainly in fertilizer industry, paint industry and also food industry to produce hydrogenated vegetable oil (Liu et al., 2014). The side product of CO_2 reforming is carbon monoxide, CO and CO can be used for production of alcohol (Li et al., 2015). On the other hand, CO_2 reforming has an important industrial advantage because natural gas normally contains CO_2 as well as C1 and some higher hydrocarbons. As a result, with CO_2 reforming, natural gas can be fed directly to the reformer unit. The literature describes many applications of CO_2 reforming such as thermo-chemical heat-pipe, production of methanol and DME (dimethyl ether) and production of an octane enhancer, methyl tertiary butyl ether (MTBE) (Albarazi et al., 2015)

2.2.6 Summary of Alternatives to Reduce CO_2 in the Atmosphere

The advantages and disadvantages of the alternative methods used to reduce CO_2 concentration in atmosphere can be summarized in Table 2.1.

Table 2.1: Alternatives used to reduce CO_2 concentration and their advantage and disadvantage.

Alternative	Advantages	Disadvantages	Reference
Monoethanolamine (MEA) scrubbing	High reactivity for even low CO_2 concentration.	High cost, consumes a lot of heat energy for solvent regeneration	Jung et al., 2013
Lime-soda process	No	High cost, high energy consumption.	Keith & Wong, 2006
Augmented ocean disposal	Does not involve complicated equipment, cost effective.	Lower the pH of water, affect marine life.	Kruger, 2010

Biochar process	Reduce the CO_2 emission from agriculture field	High cost, the effect to reduce CO_2 concentration is not significant.	Huang et al., 2015
CO_2 reforming	Clean technology eliminate CO_2 and methane from atmosphere, the major product is hydrogen gas, a useful chemical block.	No	Albarazi et al., 2015; Li et al., 2015; Liu et al., 2014

As a summary, CO_2 reforming is the best alternative to decrease the CO_2 concentration in the atmosphere. This is because it is a clean and environmental friendly alternative as it can help to eliminate two major greenhouse gases that are CO_2 and methane gas. The major product is hydrogen gas which is a useful chemical block that can be used mainly in fertilizer industry, paint industry and also food industry. The side product of CO_2 reforming is carbon monoxide, CO which can be used for production of alcohol.

2.3 CATALYST

Catalysts are defined as substances that can increase the rate of reaction by providing a pathway that will lower the activation energy of the reaction and at the same time, the catalyst can be recovered unchanged at the end of the reaction it has been used to speed up, or catalyse (Kordulis et al., 2015). For example, gaseous hydrogen and oxygen are virtually inert at room temperature but they will react rapidly when exposed to platinum catalyst. This is because in order for the reaction to happen, hydrogen and nitrogen should approach each other and pass the activation energy barrier to form the product. Activation energy is defined as the minimum amount of energy that is required to activate atoms or molecules to a condition in which they can undergo chemical transformation or physical transport (Wang et al., 2013). The activation energy barrier is

too high at room temperature so the reaction will not happen. Catalyst in this case will provide an alternative pathway that involves lower activation energy for the reaction to happen (Mutz et al., 2015). The reaction will happen rapidly since the activation energy become lower. Figure 2.1 shows the illustration on how a catalyst works to reduce the activation energy of a reaction. In brief, the catalyst will change the rate of a reaction, yield and selectivity of a reaction. Other than that, a catalyst does not affect the equilibrium position.

According the Le Chatelier's principle (Machlin & Weining, 1953), a catalyst will speed up both the forward and backward reaction to the same extent, so adding a catalyst does not affect the relative rate of the two reactions, so the equilibrium position will not be affected. A catalyst can be transition metal, transition metal oxides or enzymes. A catalyst is often used as a fine powder so that it has a bigger surface area and this will increase the catalyst activity. There are two types of catalyst that are homogeneous catalyst and heterogeneous catalyst (Karclovic & Ruiz, 2013).

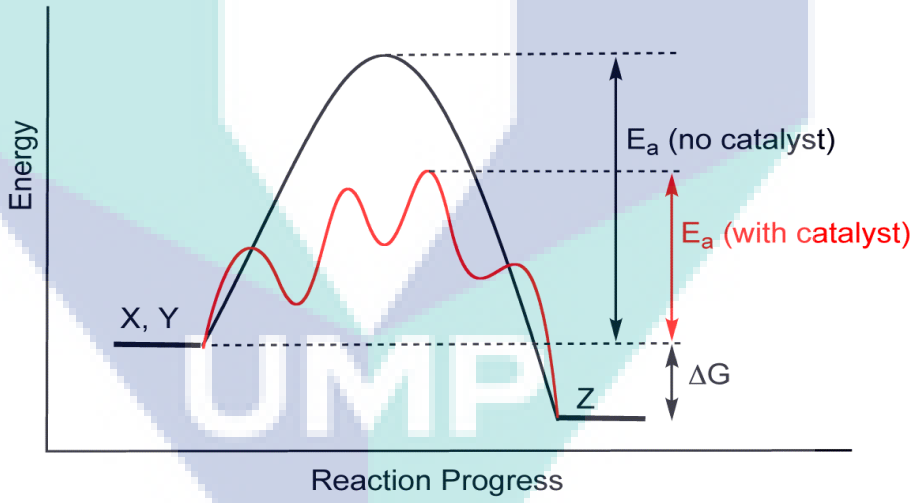

Figure 2.1: Illustration on how a catalyst works to reduce the activation energy of a reaction (Mutz et al., 2015)

The reaction of CO_2 with methane to produce hydrogen is a reaction with significant kinetic limitations, which requires a catalyst to achieve acceptable rates and selectivity for potential industrial use (Begum et al., 2015). For CO_2 reforming, heterogeneous catalyst is used rather than homogeneous catalyst. This is because heterogeneous catalysts are more stable, easy in handling, separation and reuse.

Homogeneous catalysts show satisfactory activity and selectivity, but the recovery and regeneration are problematic (Jung et al., 2013).

2.4 TYPES OF PROMOTER FOR CO_2 REFORMING

2.4.1 Ruthenium (Ru)

Jiménez et al. (2010) reported that ruthenium-promoted catalyst is the most active catalyst for CO_2 reforming due to its high activity and less coke formation. However, the drawback of ruthenium catalyst is the cost for ruthenium catalyst is too high and thus makes it not practical in industrial application (Lunde et al., 1974). In addition, according to Wang et al. (2012), when ruthenium is used as catalyst, diffusion problem is a major problem that cannot be prevented. This will decrease the rate of reaction and make the reaction become inefficient. Therefore, it can be concluded that ruthenium is not a suitable catalyst to be used for CO_2 reforming.

2.4.2 Rhodium (Rh)

Solymosi et al. (1981) studied the performance of rhodium-promoted catalyst in the CO_2 reforming. They found that rhodium-promoted catalyst has high activity, conversion and selectivity. However, Lang et al. (2015) reported that the cost for rhodium as catalyst is high and the service life of rhodium catalyst is much lower compared to other catalyst. Other than that, from the studies carried out by Harju et al. (2015), the catalyst regeneration for rhodium catalyst is problematic, difficult and expensive, and thus brings an extra cost. Thus, rhodium is not suitable to be the catalyst for CO_2 reforming.

2.4.3 Palladium (Pd), Platinum (Pt) and Molybdenum (Mo)

From the study carried out by Park et al. (2009), Palladium, Platinum and Molybdenum are used as the catalyst for CO_2 reforming. The conversion of CO_2 is low since palladium, platinum and molybdenum is not active as catalyst. Other than that, aside products that are methanol and carbon monoxide are also produced by reverse water-gas shift reaction. In addition, the catalyst regeneration for palladium, platinum

and molybdenum catalyst are complicated, problematic and expensive (Nielsen et al., 2002). So palladium, platinum and molybdenum are not suitable to be used as the catalyst for CO_2 reforming reaction.

2.4.4 Copper (Cu)

From the study carried out by Zamani et al. (2014), copper is used as the catalyst for CO_2 hydrogenation. However, CO gas is formed rather than methane gas. This is because by using copper catalyst, large amount of formate species (HCOO) which is the key intermediate for CO formation will be formed. Since CO gas is also a pollutant gas that will harm the environment, Other than that, unknown complex formation will occur when copper is used as catalyst for CO_2 reforming (Tao et al., 2010).

2.4.5 Nickel (Ni)

Previous studies (Guerrero et al., 2005; He et al., 2015; Kaydouh et al., 2015) have reported that Nickel based catalyst is the most promising catalyst which have been widely employed for reforming reaction due to their high catalytic activity, high selectivity for methane and relatively low price. Other than that, the service for Nickel catalyst is longer, the regeneration of Nickel catalyst is not problematic (Qian et al., 2014)). Apart from these, Nickel is also widely available, making it suitable for industrial application (Liu et al., 2014).

2.4.6 Summary on Types of Promoter for CO_2 Reforming

Table 2.2 shows the summary of advantages and disadvantages of various catalysts used in CO_2 reforming reaction.

Table 2.2: Catalysts used in CO_2 reforming reaction and their advantages and disadvantages

Catalyst	Advantages	Disadvantages	Reference
Ruthenium (Ru)	Catalyst activity, selectivity, and	Cost is too high.	Jiménez et al., 2010

	conversion of CO_2 are high.		
Rhodium (Rh)	Catalyst activity, selectivity and conversion of CO_2 are high.	High cost, regeneration of catalyst is difficult.	Solymosi et al., 1981
Palladium (Pd), Platinum (Pt) and Molybdenum (Mo)	No	Not active, low conversion and produce side product.	Park et al., 2009
Copper (Cu)	No	CO gas is formed rather than methane gas, CO pollute environment.	Zamani et al., 2014
Nickel (Ni)	Lower cost, lower reaction temperature, good catalytic performance and widely available	No	Aziz et al., 2015

According to Table 2.2, it can be summarized that Nickel catalyst is the most suitable catalyst for CO_2 reforming reaction because of its availability, low cost, good catalytic performance at considerable temperature.

2.5 TYPES OF SUPPORT MATERIAL FOR CO_2 REFORMING

It is widely known that the catalytic performance is greatly affected by the active surface area and the acid-base property of the catalyst support. The adsorption and dissociation of CO_2 involved in the reaction and the performance can be improved by a basic support since the CO_2 gas is an acid gas (Amin et al., 2012). Deactivation happened in the process is a major problem encountered due to the carbon deposition on

the surface, leading to blockage of reactor tubes (Amin et al., 2012). Other than coke formation, the loss of catalytic activity can also be affected by metal sintering. In this case, catalyst support will play an important role in participating in the catalytic reactivity and acting on coke resistance of the metal particles. According to Amin *et al* (2012), catalytic activity and stability are greatly influenced by support type (Amin et al., 2012). Generally, the role of the support is used to provide support for the metal catalyst materials, in order to obtain a stable and high active surface area.

2.5.1 Mesoporous Materials

Amin et al. (2012) studied on the effect of support material towards CO_2 reforming of methane. In this study, they used different types of support which are SBA-15, KIT-6, MCM-41 and SBA-15. They found that the activity of the catalyst influenced by the type of support material and the activity followed the order of Ni/SBA-15> Ni/KIT-6 > Ni/Al_2O_3> Ni/MCM-41. This activity sequence is correlated strongly with the surface area and pore diameter of these materials with the degree of CH_4 and CO_2 conversions observed. The Ni/SBA-15 which exhibited excellent catalytic performance in term of long-term stability as well as catalytic activity is the best among the mesoporous materials (Amin et al., 2012). In fact, the activity of the Ni/SBA-15 towards the degree of conversion of both CO_2 and CH_4 is much correlated to the surface area and the pore distribution (Amin et al., 2012). The Ni/SBA-15 catalyst can perform excellent catalytic performance with its more active in terms of CH_4 and CO_2 conversion than all of the other materials due to an obvious increase in the pore size, pore volume but decrease in BET surface after the Ni being introduced (Amin et al., 2012). A CH_4 conversions between 84.5 and 85.1 % and a CO_2 conversion of ~92.4 % can be performed by this type of catalyst (Amin et al., 2012). The textural properties of different samples are provided as the table below in which the catalytic performance increasing with decreasing surface area and increasing pore diameter. The Ni/SBA-15 catalyst is producing the synthesis gas with the highest H_2/CO ratios of 0.97 (Amin et al., 2012). The ability of Ni/SBA-15 catalyst to produce this high H_2/CO ratio can be explained due to reduced water gas shift reaction occurred (Amin et al., 2012). This situation takes place due to the much more rapid conversion of CO_2 on Ni/SBA-15.

Furthermore, the rate of carbon deposition on the catalysts was as follows: Ni/KIT-6 (0.0002) < Ni/ MCM-41 (0.0003) < Ni/SBA-15 (0.0005) (Amin et al., 2012).This also proves that The Ni/KIT-6 catalyst poses the lowest carbon deposition rate if compared to others two. Although MCM-41 has the lowest carbon deposition rate, yet it is very unstable at high temperatures because of the thermal deterioration (Amin et al., 2012). Mesoporous silica SBA-15 has attracted significant attention in catalysis due to its highly ordered hexagonal structure with narrow pore size distribution, thick pore wall, and high surface areas. In comparison with straight pores in MCM-41, the highly ordered two-dimensional hexagonal structure of SBA-15 is found to be much better as a support.

2.5.2 Metal Oxides Materials

Several researches have reported that the metal oxides material have a great potential to be used as support catalyst for CO_2 reforming owing to their stable physical surface, especially at high reaction temperatures. Aksoylu et al. (1996) have reported the performance of alumina (Al_2O_3) as support for CO_2 reforming. They found that Al_2O_3 performed outstanding textural and mechanical properties. Other than that, it also has relatively low cost making it applicable for industry used. However, the presence of undesirable strong metal-support interactions in the alumina-supported catalysts made it not suitable to be used as the support material of the nickel catalyst. Other than that, catalyst supported on alumina experience rapid deactivation due to the formation of $NiAl_2O_4$ which is accompany by an expansion in volume causing the shattering of the catalyst (Tan et al., 2015)

In addition, Bacariza et al. (2016) have studied the performance of titanium dioxide (TiO_2) as support for CO_2 reforming. They found that TiO_2 has few drawbacks as support materials. First, titanium dioxide has small specific surface area. This will decrease the efficiency of the catalyst since the area available for adsorption decrease. Other than that, the cost for titanium dioxide is high and this makes it not applicable in industry application. Apart from these, titanium dioxide has low quantum efficiency and low adsorption ability. It is also difficult to separate the catalyst from the reaction media and inadequate for continuous processing (Karclovic & Ruiz, 2013).

2.5.3 Summary on Types of Support Material for CO_2 Reforming

An overview of the previous studies for support materials used in CO_2 reforming is summarized in Table 2.3.

Table 2.3: Support materials used in CO_2 reforming reaction and their advantages and disadvantages

Types of Catalytic Support	Example	Advantages	Disadvantages	Author
Mesoporous	SBA-15 FSM-16 M41S family	1.Well-ordered hexagonal array structure. 2.High surface area 3.High stability 4.Highly uniform pore distribution and tunable pore size. 5 High adsorption capacity	1. Difficulty of maintaining the mesostructured of the functionalized silica materials. 2. Lack of pH stability.	Amin et al., 2012
Metal Oxides	Al_2O_3 TiO_2	1.Outstanding textural, mechanical properties and it has relatively low cost.	1. Al_2O_3-Undesirable strong metal-support interactions, cause rapid deactivation of catalyst. 2. TiO_2- Small specific surface area, high cost and low quantum efficiency and low adsorption ability.	Aksoylu et al., 1996

According to Table 2.3, it was observed that SBA-15 is the most suitable support material for Nickel catalyst since it has high surface area, well-ordered hexagonal array structure and high stability. A summary, Ni/SBA-15 catalyst has attracted much attention for CO_2 reforming of CH_4 owing to its high catalytic activity, readily available and cost effective. However, Ni/SBA-15is always accompanied by coke formation and sintering of Ni particles, which causes a severe deactivation of the catalysts. Thus, it is desirable to prepare highly dispersed Ni based catalyst which has high activity and less coke formation. In this study, effect of TEOS/P123, amount of Ni content and method of Ni loading on the properties and catalytic activity of Ni/SBA-15 were studied to obtain highly dispersed Ni/SBA-15.

CHAPTER 3

METHODOLOGY

2.1 OVERVIEW

This chapter describes the particulars of the materials and chemical reagents used in the present work, the procedure for catalyst preparation and characterization, as well as catalytic testing for CO_2 reforming of CH_4. In brief, the works are reported in four main sections:

i) Chemicals
ii) Catalyst preparation
iii) Catalyst characterization
iv) CO_2 reforming of CH_4

2.2 CHEMICALS

The chemicals used included Tetraethyl orthosilicate (TEOS), Pluronic P123, hydrochloric acid (HCl), Nickel nitrate hexahydrate ($Ni(NO_3)_2.6H_2O$), H_2 cylindrical tank, CO_2 cylindrical tank and CH_4 cylindrical tank. The list of chemicals is summarized with details in Table 3.1.

Table 3.1: List of Chemicals Used

Chemical	Purity and brand	Application
Tetraethyl orthosilicate, TEOS	99%, Merck	Catalyst preparation (Silica source)
Pluronic P123, EO_{20}-PO_{70}-EO_{20}	M_W: 5800, Aldrich	Catalyst preparation (structure directing agent)
Hydrochloric acid, HCl	37%, Merck	Catalyst preparation (pH adjustment)
Nickel Nitrate hexahydrate, $Ni(NO_3)_2.6H_2O$	99.99%, Aldrich	Catalyst preparation (Ni loading)
H_2 cylindrical tank	>99.99%	CO_2 reforming (reduction process)
CO_2 cylindrical tank	>99.99%	CO_2 reforming (Reactant)
CH_4 cylindrical tank	>99.99%	CO_2 reforming (Reactant)

2.3 CATALYST PREPARATION

2.3.1 Synthesis of SBA-15 support

The SBA-15 was prepared according to the method reported by Zhao et al. (1998). The P123 was dissolved in the solution of deionized water and 2M hydrochloric acid solution, and stirred at 40 ^oC for 1 h. The TEOS was slowly added to the mixture with vigorous stirring at 40 ^oC for 24 h, and the white precipitate product was obtained. The precipitate product was filtered, washed with deionized water and dried overnight

at 110 ^{o}C. The sample was calcined at 550 ^{o}C for 3 h to remove the triblock copolymer. For the effect of TEOS/P123 ratios, a series of samples with different mass ratios of TEOS/P123 (1.5, 2.21 and 3.0) were prepared.

2.3.2 Preparation of Ni/SBA-15

The Ni/SBA-15 catalyst was prepared by impregnation of SBA-15 powder with an aqueous solution of 5 wt% Ni salt precursor, $Ni(NO_3)_2{\cdot}6H_2O$ (Merck, 99%). The resulting slurry was heated slowly at 80 ^{o}C under continuous stirring and maintained at that temperature until all the water nearly evaporated. The solid residue was dried overnight at 110 ^{o}C followed by calcination at 550 ^{o}C for 3 h. For the effect of Ni loading, a series of sample with different Ni loading (3,5 and 10 wt%) were prepared.

For the effect of Ni-loading methods The Ni/SBA-15 catalyst was prepared by three types of preparation methods which were impregnation (IM), ion exchange (IE) and physical mixing (PM). For impregnation method, an appropriate amount of Ni salt precursor, $Ni(NO_3)_2{\cdot}6H_2O$ (Merck, 99%) was mixed with SBA-15, and then was heated slowly at 80 ^{o}C under continuous stirring and maintained at that temperature until nearly all the water had evaporated. The solid residue was dried overnight at 110 ^{o}C followed by calcination at 550 ^{o}C for 3 h to give dark grey colored Ni/SBA-15(IM). For the ion exchange method, an appropriate amount of Ni salt precursor, $Ni(NO_3)_2{\cdot}6H_2O$ (Merck, 99%) was mixed with SBA-15 under continuous stirring for 12 h. The product was filtered and dried overnight at 110 ^{o}C followed by calcination at 550 ^{o}C for 3 h to obtain Ni/SBA-15(IM). For the physical mixing method, an appropriate amount of Ni salt precursor, $Ni(NO_3)_2{\cdot}6H_2O$ (Merck, 99%) was calcined at 550 ^{o}C for 3 h to obtain black NiO powder. A desired amount of NiO was physically mixed with SBA-15 and calcined for 3 h at 550 ^{o}C to give a dark grey colored Ni/SBA-15(PM). In this study, Ni loading was adjusted at 5wt% for all catalysts.

2.4 CATALYST CHARACTERIZATION

The crystalline structure of the catalyst was determined by X-ray diffraction (XRD) recorded on powder diffractometer (Philips X' Pert MPD, 3 kW) using a Cu Kα

radiation (λ = 1.5405Å). The primary crystallite size of NiO (D_{NiO}) was calculated by means of the Scherrer equation:

$$D_{NiO} = \frac{0.9\lambda}{B\cos\theta} \quad (3.1)$$

where λ is the X-ray wavelength corresponding to Cu-Kα radiation (0.15405 nm), B is the broadening (in radians) of the nickel (200) reflection and θ is the angle of diffraction corresponding to peak broadening.

The morphologies of the samples were observed using a Scanning Electron Microscope (SEM) which will be performed using ZEISS SEM EVO-50 operating at 80kV. For the SEM measurements, the samples were dispersed in sample holder and coated at vacuum state of 50 Pa for 5 minutes before being tested.

Transmission electron microscopy (TEM) was carried out using a Philips CM12. The sample was dispersed in acetone by sonication, and deposited on an amorphous, porous carbon grid.

The Bruneuer-Emmett-Teller (BET) analysis of the catalyst was conducted using AUTOSORB-1 model AS1 MP-LP instrument at 77 K.

The Fourier Transform Infrared (FTIR) measurement was carried out using Thermo Nicolet Avatar 370 DTGS model in KBr matrix in order to study the chemical properties of catalysts and to identify the interaction of Ni species with SBA-15.

The Thermogravimetric analysis (TGA) measurement was carried out using TGA Q500,TA Instruments under a mixture of air (20%O_2/80% N_2) with heating rate of 5 $^oC\ min^{-1}$ up to 900 °C

H_2 Temperature-Programmed Reduction (H_2-TPR) analysis was carried out using Micromeritics Chemisob 2920 Pulse Chemisorption in 10% H_2/Ar at 10 $^oC\ min^{-1}$. Prior to the chemisorption, 30 mg of the catalyst was reduced with pure H_2 (20 mL

min^{-1}) at 850 ^{o}C for 1 h. The amount of hydrogen uptake was determined by injecting mixed gas (10% H_2/Ar) periodically into the reduced catalyst.

2.5 CO_2 REFORMING OF CH_4

The catalytic CO_2 reforming of CH_4 was carried out in a microcatalytic reactor at atmospheric pressure and reaction temperature of 800 ^{o}C. Prior to the reaction, 0.2 g of catalyst was reduced in a H_2 flow of 50 ml/min for 3 h at 700 ^{o}C. The feeding gas flow rate to the reactor was set at 50 ml/min, with a ratio of CH_4:CO_2:N_2 = 1:1:1, and N_2 was used as a carrier gas. The effluent gas was analyzed with an Agilent gas chromatography equipped with a thermal conductivity detector (TCD). The CH_4 and CO_2 conversion were calculated according to the following equations;

$$\text{CO}_2\ \text{Conversion}, X_{CO_2} = \frac{F_{CO_2,in} - F_{CO_2,out}}{F_{CO_2,in}} \times 100\ \% \tag{3.2}$$

$$\text{CH}_4\ \text{Conversion}, X_{CH_4} = \frac{F_{CH_4,in} - F_{CH_4,out}}{F_{CH_4,in}} \times 100\ \% \tag{3.3}$$

where F is the molar flow rate for particular compound. The product distribution ratio, H_2/CO was calculated based on equation (3.4).

$$\frac{H_2}{CO} = \frac{F_{H_2}}{F_{CO}} \tag{3.4}$$

CHAPTER 4

RESULTS AND DISCUSSION

4.1 EFFECT OF TEOS/P123 MASS RATIO ON THE PROPERTIES AND CATALYTIC ACTIVITY OF Ni/SBA-15 TOWARDS CO_2 REFORMING OF CH_4

4.1.1 Characterization of the Ni/SBA-15(R1.5), Ni/SBA-15(R2.21) and Ni/SBA-15(R3.0) Catalysts

Figure 4.1(A) shows the low-angle XRD patterns of Ni/SBA-15 with different TEOS/P123 mass ratio. The pattern of Ni/SBA-15 prepared with 2.21 TEOS/P123 mass ratio exhibited three peaks, indexed as (100), (110) and (200) which are reflection of typically two dimensional, hexagonally ordered mesostructures (*p*6mm), demonstrating the high quality of the mesopore packing (Zhao et al., 1998). When a lower (1.5) and a higher (3.0) mass ratio of TEOS/P123 were applied, the intensity of (100) peak was slightly decreased and did not feature the (110) and (200) peaks. Moreover, it was observed that the (100) peak slightly shifted to the left indicating the reduction of *d*(100) spacing and unit cell parameter. The slight decreased of (100) peak and the disappearance of the (110) and (200) peaks at lower TEOS/P123 mass ratio (TEOS/P123 = 1.5) might be due to the incomplete structural formation of SBA-15 as the amount of the TEOS was insufficient to form highly ordered hexagonal structure. Meanwhile, a reduction in the intensity of the (100) peak and the disappearance of the (110) and (200) peaks at higher TEOS/P123 mass ratio (TEOS/P123 = 3.0) might be due to a relatively poorer structural ordering of samples with a higher TEOS/P123 mass ratio because of the presence of disordered silica. The results observed in this study clearly indicated that the TEOS/P123 mass ratios (1.5 - 3.0) remarkably affected the structure of Ni/SBA-15. The changes in the XRD patterns of SBA-15 were also reported

in SBA-15 and SBA-15 PMOs for the effect of TEOS/EO-block ratio and SiO_2/P123 ratio as reported by Kruk et al. (2003) and Bao et al. (2004), respectively (Bao et al., 2004; Kruk et al., 2003). Kruk et al. (2003) found that the increasing TEOS/EO-block molar ratios (0.43 – 0.85) led to some loss of the resolution of the XRD patterns (Kruk et al., 2003). Meanwhile, Bao et al. (2004) reported that the optimum SiO_2/P123 ratio of SBA-15 PMOs was achieved at SiO_2/P123 = 72 and decreasing or increasing SiO_2/P123 ratios resulted in a decrease in the intensity of the (100) peak (Bao et al., 2004).

The presence of crystalline NiO on the catalysts was characterized using wide-angle XRD, as shown in Figure 4.1(B), in which the peaks at 37.3°, 43.2°, 62.9°, 75.4° and 79.3° can be attributed to face-centered cubic crystalline NiO structure (Aziz et al., 2015).

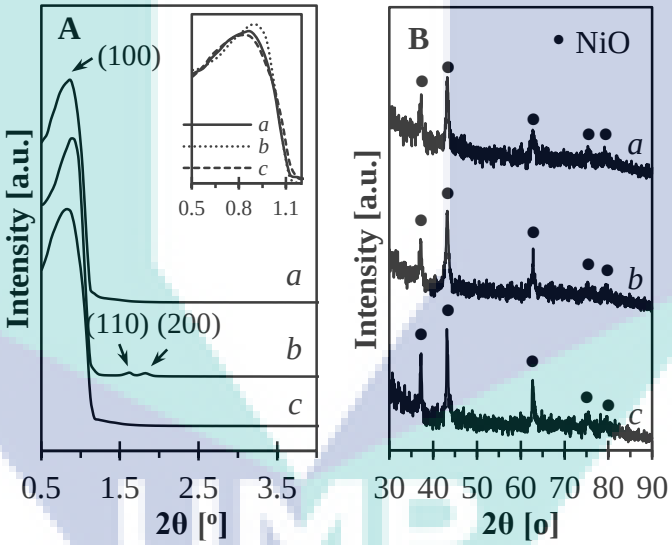

Figure 4.1: (A) Low-angle and (B) wide-angle XRD patterns of Ni/SBA-15 with TEOS/P123 mass ratios of (a) 1.5, (b) 2.21 and (c) 3.0.

An increase of TEOS/P123 mass ratio resulted in a slight increase of the peaks, suggesting that with higher TEOS/P123 mass ratio (TEOS/P123 = 3.0), most of NiO particles were aggregated on the SBA-15 outer surface, meanwhile, with lower TEOS/P123 mass ratio (TEOS/P123 = 1.5), most of NiO particles were in the SBA-15 pores. From the previous study, Lu and Kawamoto (2014) had mentioned about the influence of the synthesis method on the XRD peak intensities of NiO/SBA-15 (Lu & Kawamoto, 2014). They found that by direct synthesis method, the result showed the

higher XRD peak intensities of NiO/SBA-15 as compared to those which were prepared by post synthesis method. The result indicated that with direct synthesis method, most of the NiO particles were located on the outer surface of catalyst.

The sizes of NiO particles were calculated using the Scherrer equation and the results were 15.30, 13.42 and 22.13 nm for TEOS/P123 mass ratios of 1.5, 2.21 and 3.0, respectively. The larger size of NiO particles on TEOS/P123 = 3.0 showed the aggregation of NiO particles on the outer surface of SBA-15, in agreement with the previous assumption which stated in above discussion. It is suggested that during the assembling process, limited amount of TEOS were interacted only with the template blocks whereas the excessive amount of TEOS preferably solubilized in the copolymer micelles and condensed to form the microporous plugs. The presence of microporous plugs inhibited most of the NiO particles from entering the pores and thus they aggregated and blocked the outer surface of SBA-15.

The nitrogen adsorption-desorption isotherms of Ni/SBA-15 synthesized at different mass ratios of TEOS/P123 are shown in Figure 4.2. All samples exhibited type IV isotherm, which is a typical feature for mesoporous material, according to the IUPAC classification (Abdullah et al., 2010; Dan et al., 2012; Lu & Kawamoto, 2014)For the Ni/SBA-15 which was prepared with a TEOS/P123 mass ratio of 1.5, the isotherm exhibited a large hysteresis loop of type H3 indicating a very wide distribution of pores. However, in the case of TEOS/P123 = 2.21, the isotherm showed type H1 hysteresis loop which is a typical feature for mesoporous material which indicates a narrow distribution of relatively uniform cylindrical pores (Abdullah et al., 2010; Lu & Kawamoto, 2014). Meanwhile, when the TEOS/P123 mass ratio was further increased to 3.0, the isotherm showed type H2 hysteresis loop exhibiting non-uniform pore shapes which consisting of ill-defined pore shape and wide pore size distribution. With regards to the relative pressure, it was observed that the pore size of Ni/SBA-15 was significantly decreased with an increasing TEOS/P123 mass ratio due to the excessive amount of TEOS which could interrupt the condensation of the silica network and thus could affect pore size of the sample.

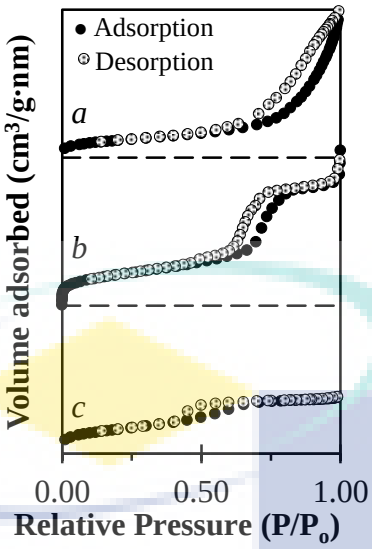

Figure 4.2: Nitrogen adsorption-desorption isotherms of Ni/SBA-15 with TEOS/P123 mass ratios of (a) 1.5, (b) 2.21 and (c) 3.0.

The surface area, pore volume and pore diameter of Ni/SBA-15 with different TEOS/P123 mass ratios are summarized in Table 4.1. With the increasing TEOS/P123 mass ratio, the surface area, pore volume and pore diameter gradually decreased. The decrease in the surface area and pore volume at higher TEOS/P123 mass ratio might be related to the excessive amount of TEOS which preferably solubilized in the copolymer micelles and condensed to form the microporous plugs. The observed trends were in a good agreement with that observed on SBA-15 and SBA-15 PMOs as reported by Kruk et al. (2003) and Bao et al. (2004), respectively (Bao et al., 2004; Kruk et al., 2003). They proposed that during the assembling process, the template blocks interacted only to a limited amount of silica source and the remaining silica source preferably solubilized in the copolymer micelles and condensed to form the microporous plugs. Meanwhile, Abdullah et al. (2010) reported that the changes in the surface area, pore volume and pore diameter of SBA-15 at higher TEOS/P123 ratio were related to the failure of Si-O-Si network formation due to the excessive amount of TEOS (Abdullah et al., 2010). Apart from that, the condensation of the silica network on the micelles might be interrupted and thus the pore structure of the sample might also be affected.

Table 4.1: Physical properties of Ni/SBA-15(R1.5), Ni/SBA-15(R2.21) and Ni/SBA-15(R3.0).

Catalyst	TEOS/123	Surface area (m^2/g)	Pore volume (cm^3/g)	Pore diameter (nm)
Ni/SBA-15(R1.5)	1.5	508	1.121	13.907
Ni/SBA-15(R2.21)	2.21	473	0.649	6.188
Ni/SBA-15(R3.0)	3.0	425	0.369	3.702

Figure 4.3 shows the influence of the TEOS/P123 mass ratio on the Ni/SBA-15 morphology structure. SEM image of Ni/SBA-15 which was synthesized from TEOS/P123 mass ratio of 1.5 showed the irregular shape of SBA-15 which might be due to the incomplete condensation stage due to the limited amount of silica source. However, in the case of TEOS/P123 mass ratio of 2.21, the SEM image showed relatively well-ordered regular shape of SBA-15 was formed. Meanwhile, when the TEOS/P123 mass ratio was further increased to 3.0, the expended and long-connecting shape with the presence of irregular shape was observed indicating poorer structural ordering of sample with partial failure in the formation of well-ordered SBA-15. In addition, it was clearly observed that most of the NiO particles were aggregated on the outer surface of Ni/SBA-15(R3.0) which in agreement with the XRD analysis. The changes in the shape of sample with template/silica ratio were also observed on ZSM-5 samples reported by Fouad et al. (2006) (Fouad et al., 2006). They found that the samples which were prepared by 0.215 and 0.322 template/silica mole ratios crystallized in cube-like shaped crystal, whereas, sample prepared by 0.43 template/silica mole ratio crystallized in sphere-like shaped crystals and the sample prepared by 0.537 template/silica mole ratio crystallized in network-like shaped crystals. The results observed in previous study clearly indicated that the different ratios of template/silica significantly affected the morphology and shape of synthesis sample.

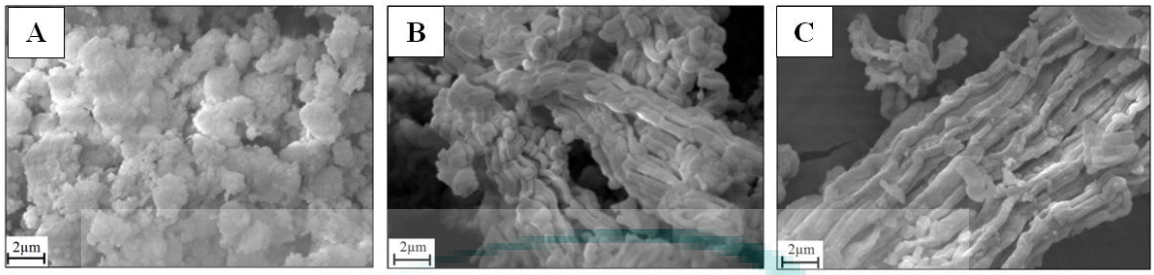

Figure 4.3: SEM images of Ni/SBA-15 with TEOS/P123 mass ratios of (A) 1.5, (B) 2.21 and (C) 3.0.

The effects of mass ratio on the structure of the sample were also confirmed by the TEM analysis as shown in Figure 4.4. The images indicated that the Ni/SBA-15 synthesized from 1.5 TEOS/P123 mass ratio showed the absence of hexagonal array because of the incomplete condensation stage of silica precursor. The condensation stage was incomplete might be due to the limited amount of silica source to interact with the excess amount of surfactant, and thus facilitate the formation of irregular shape of SBA-15. However, in the case of TEOS/P123 = 2.21, the TEM image showed relatively well-ordered hexagonal mesostructures, with microporous interconnecting hexagonal, which presented the highest ordered hexagonal mesoporous structure of SBA-15. Meanwhile, when the TEOS/P123 mass ratio was further increased to 3.0, the expended and long-connecting SBA-15 structure was observed indicating poorer structural ordering of sample at higher TEOS/P123 mass ratio. Moreover, it was observed that there was the presence of ordered and disordered silica structure in 3.0 TEOS/P123 mass ratio suggesting partially hexagonal mesoporous structure formation at higher mass ratio. This could indicate the partial failure in the formation of Si–O–Si network into hexagonal array at higher TEOS/P123 mass ratio due to the excessive TEOS amount interrupting the condensation of the silica network on the micelles. This finding was in agreement with the study reported by Abdullah et al. (2010), who found that the excess of silica precursor could affect the siloxane network structure of SBA-15 (Abdullah et al., 2010). They stated that the large amount of silica precursor interrupting the condensation of silica network on the micelles due to the limited amount of surfactant, and thus the excess silica precursor could functionalise the silica surface to form irregular silica mesopores.

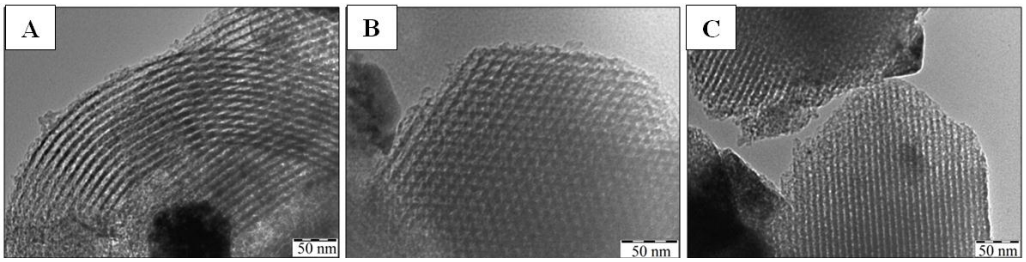

Figure 4.4: TEM images of Ni/SBA-15 with TEOS/P123 mass ratio of (A) 1.5, (B) 2.21 and (C) 3.0.

Figure 4.5 shows the FTIR spectra of KBR of Ni/SBA-15 with different TEOS/P123 mass ratios. The bands at approximately 1060, 801 and 510 cm^{-1} were corresponded to the asymmetric stretching vibrations of Si–O–Si, symmetric stretching vibrations of Si–O–Si, and tetrahedral bending vibration of Si–O–Si bonds, respectively (Fan et al., 2015; Setiabudi et al., 2016; Ye et al., 2011). It was observed that the intensity of the band at 1060 cm^{-1} was moderately decreased at higher TEOS/P123 mass ratio indicating the partial failure in the formation of Si–O–Si network at higher mass ratio due to the excessive TEOS amount interrupting the condensation of the silica network on the micelles. Based on the previous study (Brodie-Linder et al., 2010), the band around 961 cm^{-1} has been widely use to characterize the incorporation of metal ions in the silica framework in which the interaction of Ni particles with support was indicated by a decrease in the intensity of the peak and the peak becomes enveloped in the band of 1060 cm^{-1}. It was observed that incorporation of metal ions in the silica framework was following the order of Ni/SBA-15(R1.5) ≈ Ni/SBA-15(R3.0) < Ni/SBA-15(R2.21) indicating higher quantity of metal-support interaction in Ni/SBA-15 with TEOS/P123 = 2.21. At higher wavenumber, the broad adsorption band at 3440 cm^{-1} was attributed to the O-H stretching vibration mode of Si-OH involved in the hydrogen interaction with the adsorbed water molecules. An increase of TEOS/P123 mass ratios from 1.5 to 3.0 resulted in an increased of the peak, indicating higher amount of hydroxyl groups at higher TEOS/P123 mass ratio.

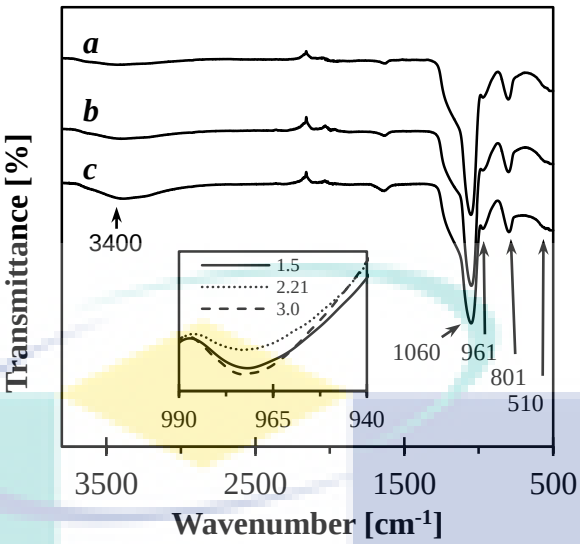

Figure 4.5: FTIR spectra of KBr of Ni/SBA-15 with TEOS/P123 mass ratio of (a) 1.5, (b) 2.21 and (c) 3.0.

4.1.2 Catalytic Performance of the Ni/SBA-15(R1.5), Ni/SBA-15(R2.21), Ni/SBA-15(R3.0) Catalysts

Figure 4.6(A) shows the effects of TEOS/P123 mass ratios on the conversion of CH_4 and CO_2 in CO_2 reforming of CH_4 at 800 ^oC for 5 h. At temperature studied, the result indicated that the highest activity and stability of Ni/SBA-15 were observed on TEOS/P123 = 2.21, while the lowest activity and stability were observed on TEOS/P123 = 1.5. The effects of TEOS/P123 mass ratios on the CH_4 conversion, CO_2 conversion and H_2/CO ratio over Ni/SBA-15 catalysts were more clearly seen in Figure 4.6(B), in which the average of CH_4 conversion, CO_2 conversion and H_2/CO ratio for 5 h were plotted as a function of TEOS/P123 ratio. The catalytic activity of Ni/SBA-15 towards CO_2 reforming of CH_4 followed the order of Ni/SBA-15(R2.21) > Ni/SBA-15(R3.0) > Ni/SBA-15(R1.5). The Ni/SBA-15(R2.21) exhibited an excellent performance with the conversion of CH_4 and CO_2 were about 89% and 88%, respectively and H_2/CO ratio of 1.02. The superior catalytic behavior of Ni/SBA-15(R2.21) might be related with the well-ordered hexagonal structure of SBA-15 which provided better dispersion of Ni particles and thus resulted in higher catalytic performance. Meanwhile, the lowest catalytic performance of Ni/SBA-15(R1.5) might be related with the incomplete hexagonal structure of SBA-15 which resulted in poorer dispersion of Ni particles as supported by the characterization results. Thus, the results

clearly indicated that TEOS/P123 mass ratio of 2.21 was the optimal synthesis ratio under the reaction studied.

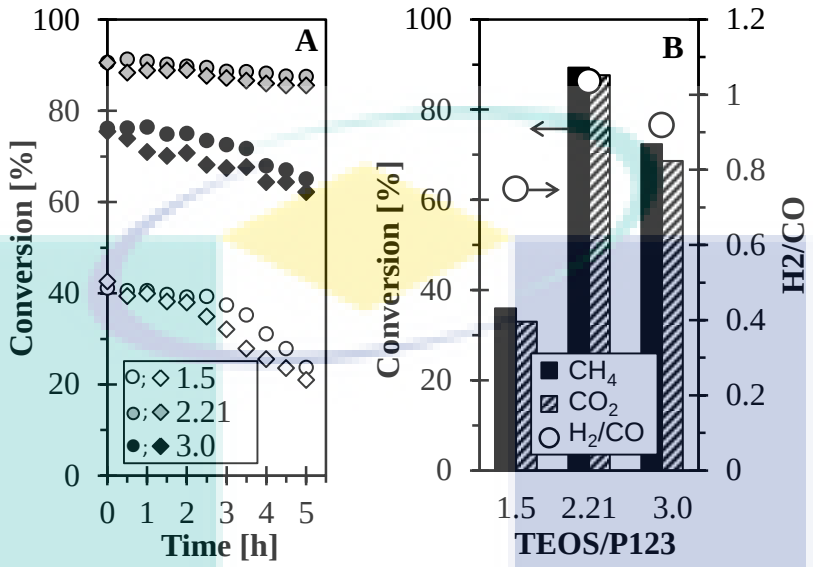

Figure 4.6: (A) CH_4 conversion (circle marker) and CO_2 conversion (diamond marker) of Ni/SBA-15 with different TEOS/P123 mass ratios (1.5, 2.21 and 3.0). (B) Effect of TEOS/P123 mass ratios on the CH_4 conversion, CO_2 conversion and H_2/CO ratio. Reaction conditions: m_{cat} = 0.2 g, F = 50 ml/min, CH_4:CO_2:N_2=1:1:1, T = 800 ^oC, P = 1 atm.

Several research groups also reported that the dispersion of metal particles on the surface of catalyst played a vital factor in enhancing the CO_2 reforming of CH_4. Sidik et al. (2016) studied on the effects of Ni-loading methods on the CO_2 reforming of CH_4. They found that the excellent catalytic activity of Ni/MSN prepared by in-situ electrolysis is closely associated with the availability of a great number of exposed Ni sites due to the high dispersion of Ni particles on the surface of catalyst. Moreover, Liu et al. (2015) found that the Ni/SBA-15 modified with the α- and γ-cyclodextrin have better catalytic performance in CO_2 reforming of CH_4 as compared to unmodified Ni/SBA-15 due to the better dispersion of Ni particles, which accessible for the reactant molecules to perform the reaction. According to the literature (Haghighi et al., 2007), CO_2 reforming of CH_4 proceed with the stepwise adsorption of CH_4 followed by the decomposition of CH_4 into CH_x fragments occur on the active metal sites, while CO_2 activation occurs mainly over the support. Thus, it is reasonable to relate the activity of catalyst with the dispersion of the metal sites on the surface of catalyst.

It is also well known that the metal-based catalysts could be easily deactivated by the deposition of cokes on the active centers of the catalysts that occurs through the Boudouard reaction ($2CO \leftrightarrow C_{(s)} + CO_2$) and/or CH_4 cracking ($CH_4 \leftrightarrow C + 2H_2$) (Haghighi et al., 2007). In this study, a quantitative analysis of carbon formation over spent Ni/SBA-15 was investigated by using TGA analysis and the results were shown in Figure 4.7. The weight loss at temperature lower than 200 ^{o}C was ascribed to the removal of adsorbed water, whereas the weight loss higher than 400 ^{o}C arose from the oxidation of carbon (Liu et al., 2015). For all catalysts, the weight loss of the carbon residuals followed a two-stage pattern at temperature below 600 ^{o}C and higher than 600 ^{o}C. The weight loss below 600 ^{o}C is associated to the oxidation of amorphous carbon, while the weight loss at higher temperature (above 600 ^{o}C) is assigned to the oxidation of graphitic carbon (Dan et al., 2012).

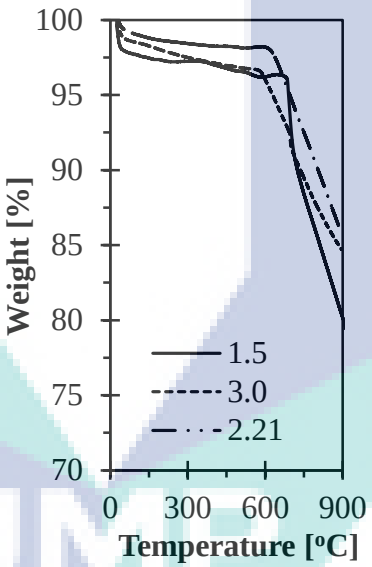

Figure 4.7: TGA curves of spent Ni/SBA-15 with TEOS/P123 mass ratio of 1.5, 2.21 and 3.0.

The amount of carbon formed in each catalyst is shown in Table 4.2. The table clearly shows that the amount of carbon formation followed the order of Ni/SBA-15(R1.5) > Ni/SBA-15(R3.0) > Ni/SBA-15(R2.21), which is in very good agreement with the decreased in the stability of the catalysts during the catalytic performance. The higher amount of the coke formation in Ni/SBA-15(R1.5) might be related with the incomplete hexagonal structure of SBA-15 which resulted in poorer Ni dispersion and thus higher deposition of cokes. The importance of the texture properties of the support

on the catalytic performance of CO_2 reforming of CH_4 was also reported by Junke et al. (2009) for $Ni/La_2O_3/Al_2O_3$ catalysts. They found that the good texture properties of support could enhance the dispersion of metal particles, improved the catalyst activity, reduced the carbon deposition, and increased the catalyst stability.

Table 4.2: Amount of carbon formed of spent Ni/SBA-15(R1.5), Ni/SBA-15(R2.21) and Ni/SBA-15(R3.0).

Catalyst	TEOS/P123	Amount of carbon (%)
Ni/SBA-15(R1.5)	1.5	17.66
Ni/SBA-15(R2.21)	2.21	12.42
Ni/SBA-15(R3.0)	3.0	12.45

4.1.3 Summary on the Effect of TEOS/P123 Mass Ratio on the Properties and Catalytic Activity of Ni/SBA-15 towards CO_2 Reforming of CH_4

The influences of TEOS/P123 mass ratios (1.5, 2.21 and 3.0) on the properties and catalytic activity of Ni/SBA-15 towards CO_2 reforming of CH_4 were studied, owing to the fact that TEOS/P123 has a significant influence on the morphology, metal-support interaction and catalytic performance of the catalyst. XRD, BET, SEM and TEM results indicated that the TEOS/P123 ratio of 2.21 was the optimal synthesis ratio of Ni/SBA-15 which producing the well-ordered hexagonal mesoporous structure with the highest Ni-support interaction. The catalytic activity of Ni/SBA-15 towards CO_2 reforming of CH_4 followed the order of Ni/SBA-15(R2.21) > Ni/SBA-15(R3.0) > Ni/SBA-15(R1.5), with the conversion of CH_4 and CO_2 over Ni/SBA-15(R2.21) was about 89% and 88%, respectively and H_2/CO ratio of 1.02. The superior catalytic behavior of Ni/SBA-15(R2.21) towards CO_2 reforming of CH_4 was related with the catalytically favorable textural properties of Ni/SBA-15(R2.21) which enhanced the dispersion of metal particles, improved the catalyst activity, increased the catalyst stability and reduced the carbon deposition. Meanwhile, the lowest catalytic performance of Ni/SBA-15(R1.5) might be related with the incomplete hexagonal structure of SBA-15 which resulted in poorer dispersion of Ni particles as supported by the characterization results. Thus, the present study confirmed that TEOS/P123 mass

ratio played as an important role in the enhancement of Ni/SBA-15 catalysts properties and catalytic performance towards CO_2 reforming of CH_4.

Since the Ni/SBA-15 with 2.21 TEOS/P123 ratio showed highest activity towards CO_2 reforming of CH_4, this ratio was used in the subsequent study.

4.2 EFFECT OF Ni LOADING ON THE PROPERTIES AND CATALYTIC ACTIVITY OF Ni/SBA-15 TOWARDS CO_2 REFORMING OF CH_4

4.2.1 Characterization of the 3Ni/SBA-15, 5Ni/SBA-15 and 10Ni/SBA-15 Catalysts

Figure 4.8(A) shows the low-angle XRD patterns of SBA-15 and Ni/SBA-15 catalysts. The patterns exhibited three peaks, indexed as (100), (110) and (200) which are reflections of typical two dimensional, hexagonally ordered mesostructures (*p*6mm), demonstrating the high quality of the mesopore packing (Zhao et al., 1998). An increase of the Ni content from 3 to 10 wt% resulted in a slight decrease of the peaks, indicating structural degradation of SBA-15. The changes in the XRD peaks are more clearly seen by calculating the percentage crystallinity of the catalysts as shown in Table 4.3. The percentage crystallinity of SBA-15 was decreased from 100% to 85.4% with the introduction of Ni species (3 – 10 wt%), indicating the partial collapse of structure with the presence of Ni. The presences of Ni crystallites on the surface of catalysts were characterized using wide-angle XRD, as shown in Figure 4.8(B). The peaks assigned to face-centered cubic crystalline NiO at 37.3^o, 43.2^o, 62.9^o, 75.4^o and 79.3^o (Aziz et al., 2015)were more intense with increasing Ni loading, in agreement with more crystalline phase of NiO on the SBA-15.

The textural properties of all catalysts are summarized in Table 4.3. For bare SBA-15, the BET surface area was 856 m^2/g with pore volume of 0.999 cm^3/g. However, the introduction of Ni from 3 to 10 wt% decreased the surface area and pore volume of SBA-15, indicating the blockage of the pores by Ni species. It is noted that the particles size of Ni species significantly increased with 10 wt% of Ni content might due to the agglomeration of Ni particles at higher amount of metal loading. Moreover, 10Ni/SBA-15 has slightly higher pore volume than 5Ni/SBA-15 which indicative of metal particle agglomeration leading to a slight contraction of the walls and

consequently expansion of the pores. The change in the BET surface area of the catalyst caused by the different amounts of metal loading was also observed for Ni/MSN and Co/SBA-15 catalysts, reported by Aziz et al. (2015) and Martínez et al. (2003), respectively (Aziz et al., 2015; Martínez et al., 2003). They found that increasing the amount of metal loading resulted to a decrease in the surface area of the support catalyst due to the blockage of the pores with metal species. Moreover, the presence of larger metal particles at higher amount of metal loading due to the agglomeration of metal particles was also reported for the same catalysts.

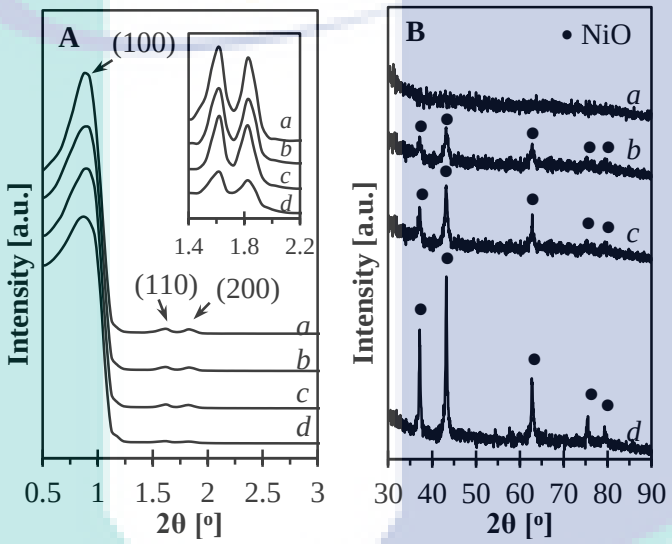

Figure 4.8: (A) Low and (B) wide angle XRD patterns of (a) SBA-15, (b) 3Ni/SBA-15, (c) 5Ni/SBA-15 and (d) 10Ni/SBA-15.

Table 4.3**:** Physical properties of SBA-15, 3Ni/SBA-15, 5Ni/SBA-15 and 10Ni/SBA-15.

Catalyst	Nickel content (wt%)	XRD crystallinity (%)	BET Surface Area (m^2/g)	Pore volume (cm^3/g)	Ni particle size (nm)[a]
SBA-15	0	100	856	0.999	-
3Ni/SBA-15	3	93.2	650	0.728	10.7
5Ni/SBA-15	5	91.3	473	0.649	13.6
10Ni/SBA-15	10	85.4	329	0.699	25.9

[a] Determine by XRD (Scherer equation)

The agglomeration of Ni particles at higher metal loading was investigated using TEM, as shown in Figure 4.9, in which the presence of Ni particles was observed by the occurrence of small spots with darker contrast areas. The 5Ni/SBA-15 catalyst showed the deposition of small Ni particles, whereas 10Ni/SBA-15 was contain of large-sized Ni particles due to the agglomeration of Ni particles at higher amount of Ni loading. In accordance with the XRD and BET results, it is believed that the higher amount of Ni loading will lead to agglomeration of Ni particles and thus increase the size of Ni particles.

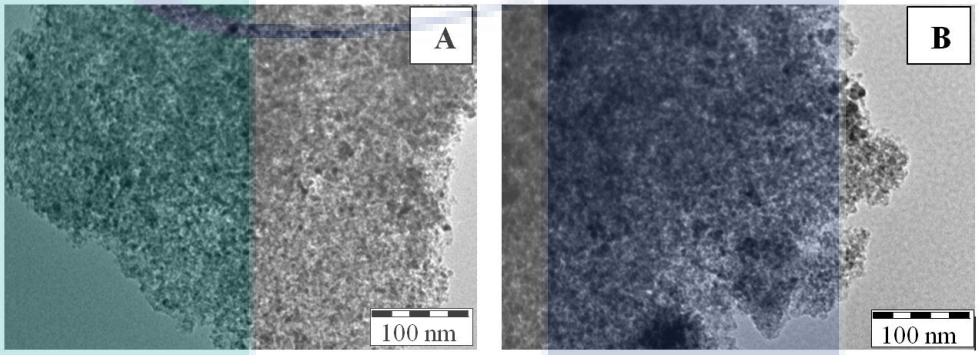

Figure 4.9: TEM images of (A) 5Ni/SBA-15 and (B) 10Ni/SBA-15.

Figure 4.10 shows the FTIR spectra of KBr in the range of 1400 – 500 cm^{-1} and 3800 – 2500 cm^{-1}. The bands in the range of 1400 and 500 cm^{-1} are attributed to the vibrations of the stretching and bending modes of Si-O units, while the bands in the range of 3800 and 2500 cm^{-1} are associated with O-H stretching vibration mode of Si-OH involved in hydrogen interaction with the adsorbed water molecules. The bands at approximately 1060 and 801 cm^{-1} corresponded to the asymmetric and symmetric stretching vibrations of Si–O–Si in the framework, respectively (Chanadee & Chaiyarat, 2016). Meanwhile, the band at approximately 961 and 510 cm^{-1} corresponded to the Si–O stretching vibration of Si–OH groups and tetrahedral bending vibration of Si–O–Si bonds, respectively (Brodie-Linder et al., 2010)

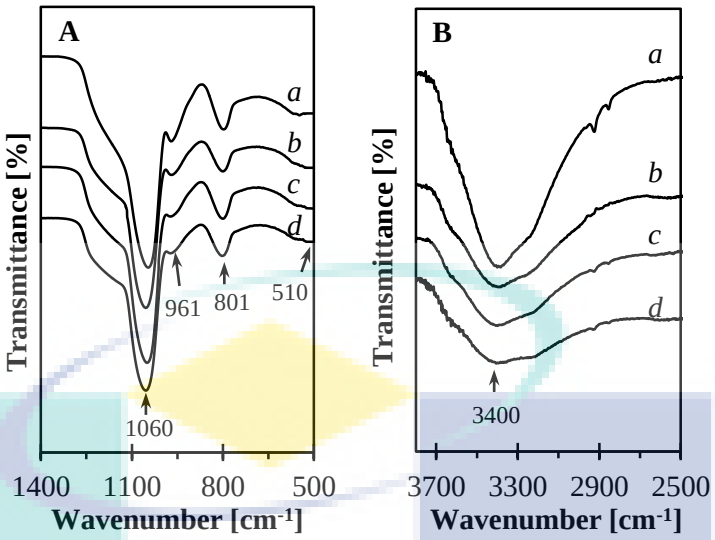

Figure 4.10: FTIR spectra of KBr in the range of (A) 1400 – 500 cm^{-1} and (B) 3800 – 2500 cm^{-1} of (a) SBA-15, (b) 3Ni/SBA-15, (c) 5Ni/SBA-15 and (d) 10Ni/SBA-15.

The introduction of Ni on SBA-15 did not alter the intensities of the bands at 1060, 801 and 510 cm^{-1} indicating neither asymmetric stretching, symmetric stretching nor tetrahedral bending of Si-O-Si interacted with Ni. However, the intensity of the band at 961 cm^{-1} decreased slightly and becomes enveloped in the peak of 1060 cm^{-1} indicating the formation of Ni–O bonds replacing the hydrogen atoms of Si–OH. Moreover, it was observed that an increase in Ni loading decreased the intensity of O–H stretching vibration mode of Si–OH involved in hydrogen interaction with the adsorbed water molecules at 3400 cm^{-1}, indicating the substitution of O–H with O–Ni. Therefore, the changes in the intensities of the bands at 3400 and 961 cm^{-1} are considered as a direct evidence for the formation of Si–O–Ni by substitution of O–H with O–Ni. The change of the SBA-15 structure caused by the introduction of metal was also observed on the Cu-SBA-15 catalyst reported by Brodie-Linder et al. (2010) (Brodie-Linder. et al., 2010). They found that the intensity of the band assigned to Si–O stretching vibration of the Si–OH groups at 960 cm^{-1} disappears and becomes enveloped in the large Si–O framework peak at 1068 cm^{-1} owing to the formation of Cu–O bonds.

Figure 4.11 shows the TGA curves of SBA-15 and Ni/SBA-15 catalysts. The TGA results explained the phenomenon of weight loss, which results from heating the samples in a mixture of N_2 and O_2 flow. The curves of all catalyst showed a weight loss region in the range of 27 to 200 ^oC, indicating the loss of catalyst water content. The

weight loss percentage was less significant with the introduction of Ni, indicating the reduction of catalyst water content in the presence of Ni. This result was related with the substitution of surface silanol groups with Ni species, which indirectly eliminated the hydrogen interaction between silanols and adsorbed water molecules. The weight loss percentage was decreased with an increase in Ni loading (3 – 5 wt%), and no further decreased was observed with increasing amount of Ni loading (up to 10 wt%). This result indicated that the maximum substitution of surface silanol groups with Ni species was achieved at 5 wt%, and further increase in Ni loading stimulate the agglomeration of Ni particles. Moreover, it was observed that none of the catalyst experienced the formation of intermediate compound upon increasing the temperature, indicating that all catalyst were thermally stable at high temperatures. The change of the weight loss percentage caused by the introduction of metal was also observed on the Ir-HZSM-5 (Setiabudi et al., 2011)in which the weight loss of water was less pronounced when the HZSM-5 contains Ir.

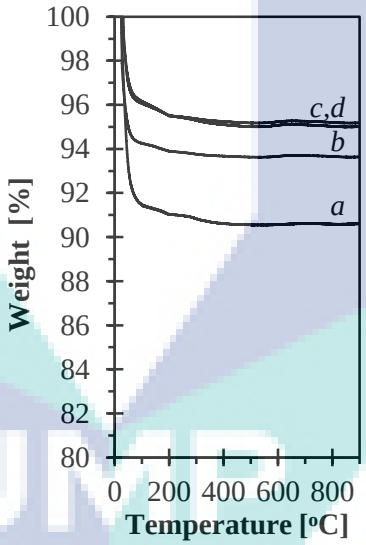

Figure 4.11: TGA curves of (a) SBA-15, (b) 3Ni/SBA-15, (c) 5Ni/SBA-15 and (d) 10Ni/SBA-15.

Figure 4.12 shows the TPR profile of the Ni/SBA-15 catalysts with various Ni loadings. In the case of 3Ni/SBA-15 and 5Ni/SBA-15, the deconvoluted TPR profile consists of four peaks centered at 380, 438, 490 and 540 ^{o}C. Meanwhile, the deconvoluted TPR profile of 10Ni/SBA-15 consists of four peaks centered at 380, 418, 460 and 520 ^{o}C. The decrease in the temperature of TPR peaks at 10Ni/SBA-15 might be due to the presence of agglomerate NiO particles which can easily migrate and

aggregate during the reduction process. According to the Sidik et al. (2016) (Sidik et al., 2016), the peaks in the low temperature zone (< 400 ^{o}C) are assigned to the reduction of Ni_2O_3 or NiO species, while the peaks in temperature higher than 400 ^{o}C are assigned to the reduction of NiO species which interacted with the support. In brief, the peaks in the medium temperature zone (400 to 500 ^{o}C) are assigned to the reduction of NiO species which have weak interaction with the support, while the peaks in the high temperature zone (500 to 600 ^{o}C) are assigned to the reduction of NiO species having medium strength interaction with the support (Oemar et al., 2016)

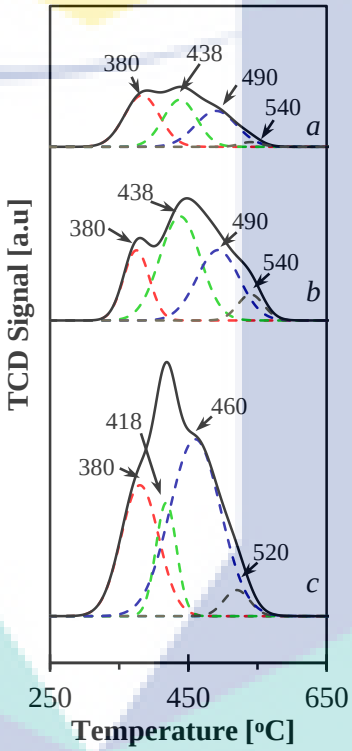

Figure 4.12: H_2-TPR profiles of (a) 3Ni/SBA-15, (b) 5Ni/SBA-15 and (c) 10Ni/SBA-15. The dotted line represents the Gaussian peaks.

The TPR data are categorized based on the temperature zone and the data are presented in Table 4.4. Based on the summarized information in Table 4.4, it was observed that an increase in Ni loading (up to 5 wt%) substantially increase the peak area of medium and high temperature zone, indicating the positive role of Ni in promoting the metal-support interaction. However, a further increase in the Ni loading from 5 to 10 wt% resulted in a significant increase in the peak area of low and medium temperature zone without changing the peak area of high temperature zone, indicating a dramatic increase in the amount of un-bound and weakly bound NiO species with the same amount of medium strength of NiO interaction. This result shows that the

formation of medium strength of NiO interaction (Ni-O-Si) through the substitution of surface silanol groups with Ni species was achieved the maximum at 5 wt% and further increase in Ni loading stimulate the agglomeration of Ni particles which can easily migrate and aggregate during the reduction process.

Table 4.4: Deconvoluted H_2-TPR analysis of 3Ni/SBA-15, 5Ni/SBA-15 and 10Ni/SBA-15.

Catalyst	Peak Area		
	< 400 ^oC (low)	400 – 500 ^oC (medium)	500 – 600 ^oC (high)
3Ni/SBA-15	0.4643	0.7867	0.0268
5Ni/SBA-15	0.4646	1.8514	0.1736
10Ni/SBA-15	1.2618	2.8993	0.1736

.

4.2.2 Catalytic Performance of the 3Ni/SBA-15, 5Ni/SBA-15 and 10Ni/SBA-15 Catalysts

Figure 4.13(A) and Figure 4.13(B) show the effect of Ni loading on the conversion of CH_4 and CO_2 in CO_2 reforming of CH_4 at 800 ^oC. The reaction of bare SBA-15 showed lower activity (< 5% of CO_2 and CH_4 conversion), indicating that the metallic sites are necessary in the studied catalytic reaction. At temperature studied, 5Ni/SBA-15 exhibited an excellent performance with the highest stability as compared to 3Ni/SBA-15 and 10Ni/SBA-15. The effect of Ni loading on the performance of Ni/SBA-15 towards CO_2 reforming of CH_4 is more clearly illustrated in Figure 4.13(C), in which the average of CH_4 conversion, CO_2 conversion and H_2/CO ratio were plotted as a function of Ni loading. The catalytic activity of Ni/SBA-15 towards CO_2 reforming of CH_4 followed the order of 5Ni/SBA-15 > 3Ni/SBA-15 ≈ 10Ni/SBA-15, whereas the average H_2/CO ratio followed the order of 5Ni/SBA-15 > 3Ni/SBA-15 > 10Ni/SBA-15. The 5Ni/SBA-15 catalyst exhibited an excellent performance with the conversion of CH_4 and CO_2 was about 89% and 88%, respectively and H_2/CO ratio of 1.02. The superior catalytic behavior of 5Ni/SBA-15 towards CO_2 reforming of CH_4 probably was related to the substitution of surface silanol groups with Ni species, which altered the

properties of catalyst towards an excellent catalytic performance. Meanwhile, a decreased in the catalytic performance with further increase in Ni loading (10 wt%) might be related to the agglomeration of Ni particles on the surface of SBA-15. The change in the activity of catalyst with metal loading was also observed on the Ni/CeO_2/MgO catalyst, as reported by Khajenoori et al. (2015) (Khajenoori et al., 2015). They found that the increasing in Ni loading up to 10 wt% increased the conversion of CH_4 and CO_2, while, further increasing in Ni content more than 10 wt% decreased the activity of catalyst due to an increase in the Ni crystallite size at higher Ni loading. In addition, Sidik et al. (2016) found that the higher catalytic properties of Ni/MSN is attributed to the strongest Ni-support interaction, while the lower catalytic activity of Ni/MSN is attributed to the inferior dispersion of Ni species as well as the larger Ni particles size arose from the weaker Ni-support interaction (Sidik et al., 2016). Moreover, Rahemi et al. (2014) also found that the dispersion and crystallite size of metal are vital factors in enhancing the catalytic activity of the catalyst (Rahemi et al., 2014). Based on this information, it can be assumed that the excellent catalytic activity of 5Ni/SBA-15 is closely related with the better dispersion of Ni particles on the surface of catalyst owing to the existence of the metal-support interaction (Si–O–Ni).

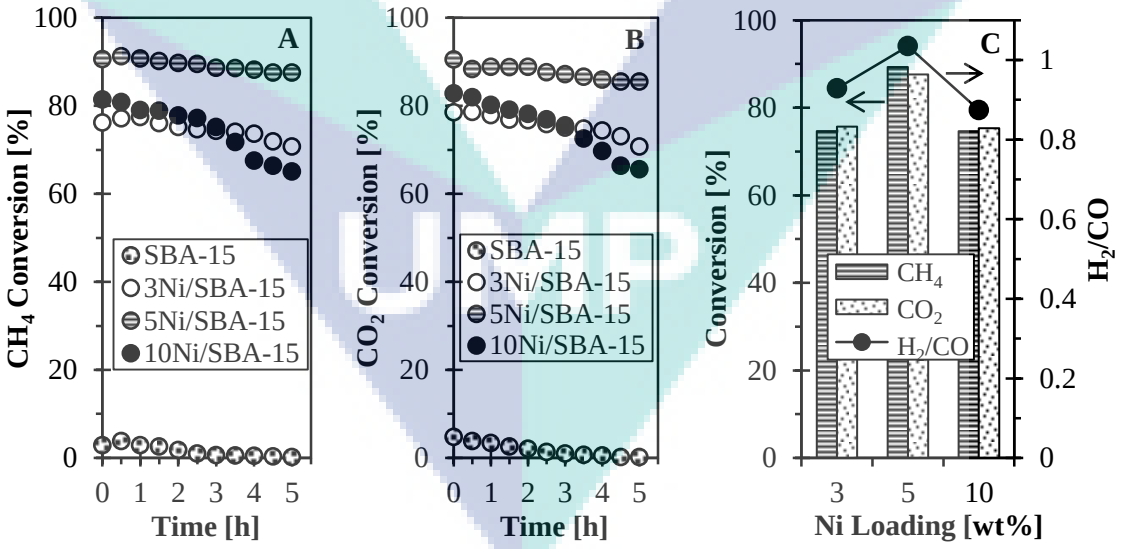

Figure 4.13: (A) CH_4 conversion and (B) CO_2 conversion of SBA-15, 3Ni/SBA-15, 5Ni/SBA-15 and 10Ni/SBA-15 in CO2 reforming of CH4. (C) Effect of Ni loading on the CH_4 conversion, CO_2 conversion and H_2/CO ratio. Reaction conditions: m_{cat} = 0.2 g, F = 50 ml/min, CH_4:CO_2:N_2=1:1:1, T = 800 ^oC, P = 1 atm.

According to the proposed mechanism for CO_2 reforming of CH_4, the stepwise adsorption of CH_4 followed by its decomposition into CH_x fragments occurs on active metal sites, whereas CO_2 activation occurs mainly over the supports (Vafaeian et al., 2013). Based on this information, it can be assumed that the excellent activity of 5Ni/SBA-15 is closely associated with the substitution of surface silanol groups with Ni species, which enhanced the stabilization of the active Ni species on SBA-15 support and altered the properties of catalyst towards an excellent catalytic performance. The relation of metal-support interactions with CO2 reforming of CH_4 was also observed in TiO_x/Pt catalysts reported by Bradford and Vannice (1997). They found that the active sites for the CO_2 reforming of CH_4 are created in the metal-support interfacial region which promotes CH_4 dissociation and CO_2 dissociation. In addition, Sidik et al. (2016) found that the higher catalytic activity of Ni/MSN towards CO_2 reforming of CH_4 was associated with the availability of a great number of active sites arose from the strong interaction between the Ni and the support (Sidik et al., 2016). By referring to the previous studies, it is reasonable to conclude that the metal-support interaction (Si–O–Ni) are responsible for the formation of active sites, and thus resulted in higher catalytic performance.

4.2.3 Characterization of the spent 3Ni/SBA-15, 5Ni/SBA-15 and 10Ni/SBA-15 Catalysts

A quantitative analysis of carbon formation over the spent Ni/SBA-15 after 5 h reaction was investigated by TGA analysis and the results are shown in Figure 4.14. For all catalysts, the weight loss of the carbon residuals followed a two-stage pattern, a first one that slowly develops a broad reduction at 300 to 500 ^{o}C, and another one at temperature higher than 500 ^{o}C. According to the previous report (Son et al., 2014), the oxidation of amorphous species occurs at low temperature (400 – 500 ^{o}C), while graphite carbon is oxidized at higher temperature (above 500 ^{o}C). Thus, the amount of carbon deposited on the surface of catalysts was quantified based on the percentage weight loss from 400 ^{o}C and above. Based on the calculation, the amount of carbon content followed the order of 5Ni/SBA-15 (10.8%) < 3Ni/SBA-15 (13.3%) < 10Ni/SBA-15 (21.7%). It is evident that 5wt% Ni loading have lower amount of carbon deposition compared to the 3 wt% and 10 wt% Ni loading. This result can be explained by the presence metal-support interaction which prevents the Ni particle being carried

away from the SBA-15 surface, thus minimizing the growth of encapsulating graphite carbon.

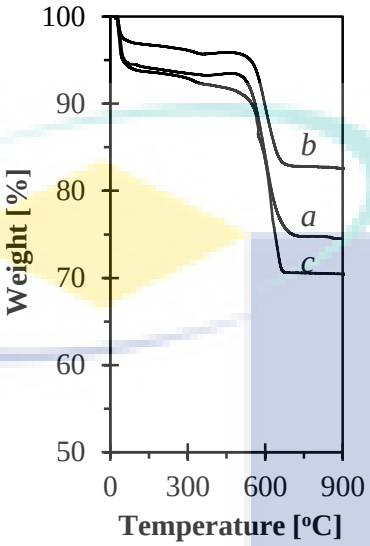

Figure 4.14: TGA curves of (a) spent 3Ni/SBA-15, (b) spent 5Ni/SBA-15 and (c) spent 10Ni/SBA-15 after 5 h reaction.

4.2.4 Summary on the Effect of Ni Loading on the Properties and Catalytic Activity of Ni/SBA-15 towards CO_2 Reforming of CH_4

The influences of Ni loading (3 – 10 wt%) on the properties of Ni/SBA-15 and CO_2 reforming of CH_4 were studied, owing to the fact that metal loading has a significant influence on the metal-support interaction and catalytic performance of the catalyst. Characterization results indicated that the formation of Ni–O–Si by substitution of surface silanol groups with Ni species and the maximum substitution was achieved at 5 wt% loading, while further increase in Ni loading stimulate the agglomeration of Ni particles. The catalytic activity of Ni/SBA-15 towards CO_2 reforming of CH_4 followed the order of 5Ni/SBA-15 > 3Ni/SBA-15 ≈ 10Ni/SBA-15, whereas the average H_2/CO ratio followed the order of 5Ni/SBA-15 > 3Ni/SBA-15 > 10Ni/SBA-15. The superior catalytic behavior of 5Ni/SBA-15 towards CO_2 reforming of CH_4 probably was related to the presence of Ni–O–Si, which enhanced the stabilization of the active Ni species on SBA-15 and altered the properties of catalyst towards an excellent catalytic performance. In addition, the analysis of spent Ni/SBA-15 catalysts found that the presence of Ni–O–Si minimizes the growth of encapsulating graphite carbon and thus

enhanced the stability of catalyst. Thus, the present study confirmed that metal-support interaction, Si–O–Ni played an important role in the enhancement of the catalytic performance of Ni/SBA-15 catalysts.

Since the Ni/SBA-15 with 5 wt% showed highest activity towards CO_2 reforming of CH_4, 5 wt% Ni loading was used in the subsequent study.

4.3 EFFECT OF Ni-LOADING METHODS ON THE PROPERTIES AND CATALYTIC ACTIVITY OF Ni/SBA-15 TOWARDS CO_2 REFORMING OF CH_4

4.3.1 Characterization of the Ni/SBA-15(IM), 5Ni/SBA-15(IE) and 10Ni/SBA-15(PM) Catalysts

Figure 4.15 shows the low- and wide-angle XRD patterns of SBA-15 and Ni/SBA-15 catalysts prepared by different Ni-loading methods.

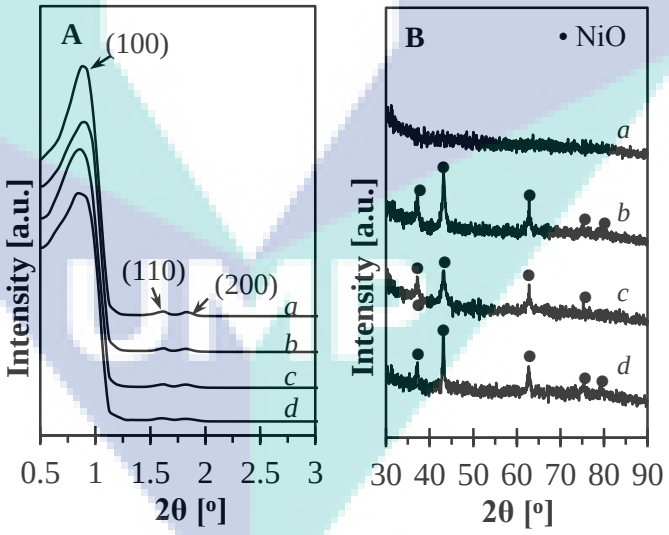

Figure 4.15: (A) Low and (B) wide angle XRD patterns of (a) SBA-15, (b) Ni/SBA-15(IM), (c) Ni/SBA-15(IE) and (d) Ni/SBA-15(PM).

As shown in Figure 4.15(A), all the catalysts showed three peaks at 2θ = 0.9, 1.6 and 1.8^o, corresponding to the (100), (110) and (200) which are reflections of typical two dimensional, hexagonally ordered mesostructures (*p*6mm), demonstrating the high

quality of the mesopores packing (Zhao et al., 1998). The introduction of Ni has decreased the intensity of the peaks, suggesting partial blocking of the mesoporous structure. The changes in the XRD peaks are more clearly seen by calculating the percentage crystallinity of catalyst as listed in Table 4.5. By comparing the effects of Ni-loading methods, it was observed that the percentage crystallinity followed the order of Ni/SBA-15(IE) > Ni/SBA-15(IM) > Ni/SBA-15(PM) indicating physical mixing method results in serious aggregation of Ni particles on the surface of SBA-15, resulting the higher blocking of the mesoporous structure.

The presence of Ni on the surface of SBA-15 was characterized using wide-angle XRD analysis and the result shown in Figure 4.15(B). The XRD patterns of Ni/SBA-15 catalysts showed several diffraction peaks for NiO at 37.3^{o}, 43.2^{o}, 62.9^{o}, 75.4^{o}, 75.4^{o} and 79.3^{o} (Sidik et al., 2016). A measurement of the NiO crystallite size was carried out using scherrer equation at $2\theta = 43.2^{o}$ and the results are shown in Table 1. As shown in Table 1, it was observed that NiO particle sizes followed the order of Ni/SBA-15(IE) < Ni/SBA-15(IM) < Ni/SBA-15(PM) indicating higher agglomeration degree of Ni/SBA-15(PM) which might due to the weaker metal-support interaction presence in the catalyst. Several research groups were also reported higher agglomeration degree of metal due to the weaker metal-support interaction including Ni/MSN(PM) (Sidik et al., 2016) and Co/SiO_2 catalysts. The higher agglomeration degree of Ni/SBA-15(PM) was confirmed by comparing the TEM images of Ni/SBA-15(IM) and Ni/SBA-15(PM) as shown in Figure 4.16, in which the presences of the Ni particles were observed by the occurrence of the spots with darker contrast areas. It was observed that the Ni/SBA-15(PM) catalyst has serious agglomeration as compared to the Ni/SBA-15(IM) catalyst. The result observed in TEM analysis was in agreement with the XRD analysis.

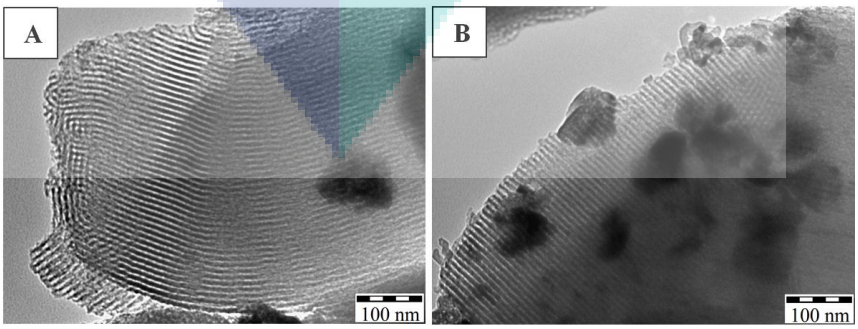

Figure 4.16: TEM images of (A) Ni/SBA-15 (IM) and (B) Ni/SBA-15 (PM).

The BET surface area and pore volume of the SBA-15 and Ni/SBA-15 catalysts are shown in Table 4.5. It was observed that the introduction of Ni by impregnation, ion exchange and physical mixing had decreased the surface area and pore volume of the catalysts from 856 m^2/g to 473, 594 and 426 m^2/g, and from 0.999 cm^3/g to 0.649, 0.623 and 0.469 cm^3/g, respectively, indicating the blockage of the pores with Ni species. The blockages of SBA-15 pores with the introduction of Ni species were also reported on the Ni/SBA-15 prepared by P123-assisted method (Wang et al., 2013)and heat treatment method (Lu & Kawamoto, 2014)

Table 4.5: Physical properties of SBA-15, Ni/SBA-15(IM), Ni/SBA-15(IE) and Ni/SBA-15(PM).

Catalyst	XRD crystallinity (%)	BET Surface Area (m^2/g)	Pore volume (cm^3/g)	Ni particle size (nm)[a]
SBA-15	100	856	0.999	-
Ni/SBA-15(IM)	91.3	473	0.649	13.6
Ni/SBA-15(IE)	94.8	594	0.623	11.6
Ni/SBA-15(PM)	89.6	426	0.469	18.5

[a] Determine by XRD (Scherer equation)

Figure 4.17 shows the FTIR spectra of KBr in the range of 1400 – 500 cm^{-1} and 3800 – 2500 cm^{-1}. For FTIR spectra in range of 1400 – 500 cm^{-1} (Figure 3(A)), there are four significant peaks observed at 1060, 961, 801 and 510 cm^{-1}, which are assigned to the asymmetric stretching Si-O-Si, Si-O stretching of Si-OH groups, symmetric stretching Si-O-Si, and tetrahedral bending of Si-O-Si, respectively (Brodie-Linder. et al., 2010). The introduction of Ni by all three methods did not alter the intensities of the peaks at 1060, 801 and 510 cm^{-1} indicating neither asymmetric stretching Si-O-Si, symmetric stretching Si-O-Si nor tetrahedral bending of Si-O-Si interacted with Ni particles. However, the intensity of the peak at 961 cm^{-1} which was assigned to Si-O stretching of Si-OH had decreased slightly and became enveloped in the peak of 1060 cm^{-1} indicating the interaction of Ni particles with support by replacing the Si-OH with Si-O-Ni. Moreover, it was observed (inset figure) that the decrease in the intensity of the peak followed the order of Ni/SBA-15(IE) > Ni/SBA-15(IM) > Ni/SBA-15(PM)

indicating that Ni/SBA-15(IE) had higher metal-support interaction as compared to other methods. The direct evidence for the formation of Si-O-Ni by substitution of O-H with O-Ni was observed in Figure 3(B). The intensity of the peak at 3400 cm^{-1} which was assigned to O-H stretching vibration mode of Si-OH involved in hydrogen interaction with the adsorbed water molecules was decreased with the order of Ni/SBA-15(IE) > Ni/SBA-15(IM) > Ni/SBA-15(PM) due to the substitution of O-H with O-Ni.

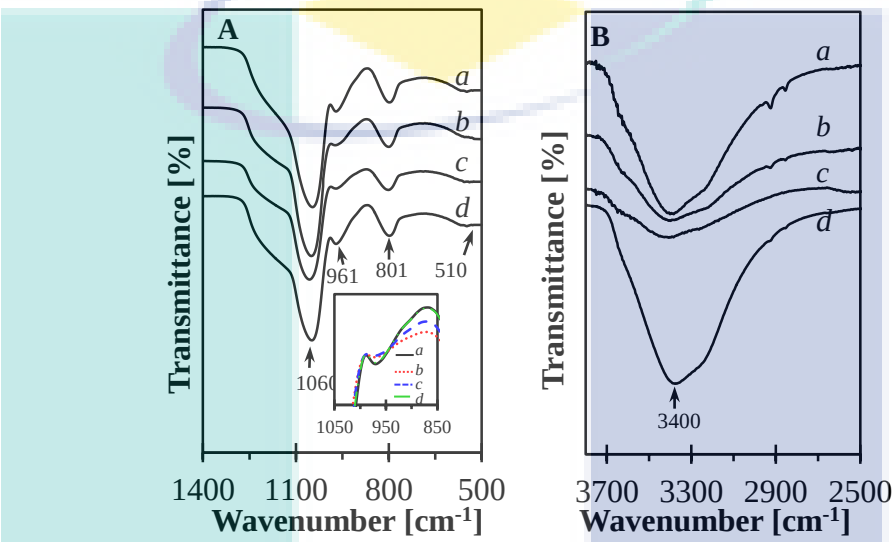

Figure 4.17: FTIR spectra of KBr in the range of (A) 1400 – 500 cm^{-1} and (B) 3800 – 2500 cm^{-1} of (a) SBA-15, (b) Ni/SBA-15(IM), (c) Ni/SBA-15(IE) and (d) Ni/SBA-15(PM).

The change of the FTIR peaks caused by the introduction of metal was also observed on Co and Cr supported SBA-15 reported by Wang et al. (2016). They found that the introduction of Cu and Cr resulted in slight red shift of the peak at 965 cm^{-1} indicating the partial metal incorporation and the formation of O-M (M is Cu(II) or Cr(VI)) type linkage. In addition, Xia et al. (2008) reported that the introduction of Co into the SBA-15 decreased the absorbance intensity of nonbridging oxygen atoms (Si-$O^{\delta-}$) of Si-OH stretch at 970 cm^{-1} implying that Si-OH groups were consumed and transformed to Si-O-Co bonds. On the basis of the literature, thus, it is reasonable to conclude that the decreased of the peak at 961 cm^{-1} was related with the formation of Ni-support interaction (Si-O-Ni) through the substitution of O-H with O-Ni.

Figure 4.18 shows the TGA curves of SBA-15 and Ni/SBA-15 catalysts prepared by different Ni-loading methods. All the catalysts showed a weight loss region in the range of 27 ^{o}C to 200 ^{o}C, indicating the loss of catalyst water content. It was observed that the introduction of Ni on SBA-15 had reduced the amount of weight loss, that might be due to the elimination of hydrogen interaction between silanols and adsorbed water molecules by the substitution of surface silanol groups with Ni species. With regards to the effects of preparation methods, the weight loss of catalysts was following the order of Ni/SBA-15(PM) > Ni/SBA-15(IM) > Ni/SBA-15(IE) indicating that Ni/SBA-15(IE) had the lowest amount of water content due to the higher amount of metal-support interaction (Si-O-Ni).

The trend observed in TGA analysis was in agreement with the FTIR analysis. A decrease in the weight loss percentage caused by the removal of OH groups through the interaction of metal with support was also observed on the Ir-HZSM5 in which the mass loss region in the range of 25 to 350 ^{o}C was less pronounced when the HZSM-5 contains Iridium (Setiabudi et al., 2011).

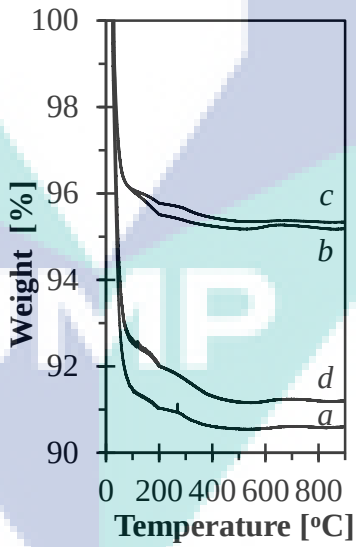

Figure 4.18: TGA curves of (a) SBA-15, (b) Ni/SBA-15(IM), (c) Ni/SBA-15(IE) and (d) Ni/SBA-15(PM).

4.3.2 Catalytic Performance of the Ni/SBA-15(IM), 5Ni/SBA-15(IE) and 10Ni/SBA-15(PM) Catalysts

Figure 4.19(A) and 4.19(B) show the conversion of CH_4 and CO_2 of SBA-15 and Ni/SBA-15 prepared by different Ni-loading methods at 800°C. The reaction of SBA-15 showed lower activity (< 5 %) indicating that Ni particles are necessary for the studied catalytic reaction. The effects of Ni-loading methods are more clearly seen by calculating the average conversion and average H_2/CO ratio for 10 h of reaction as shown in Figure 5(C).

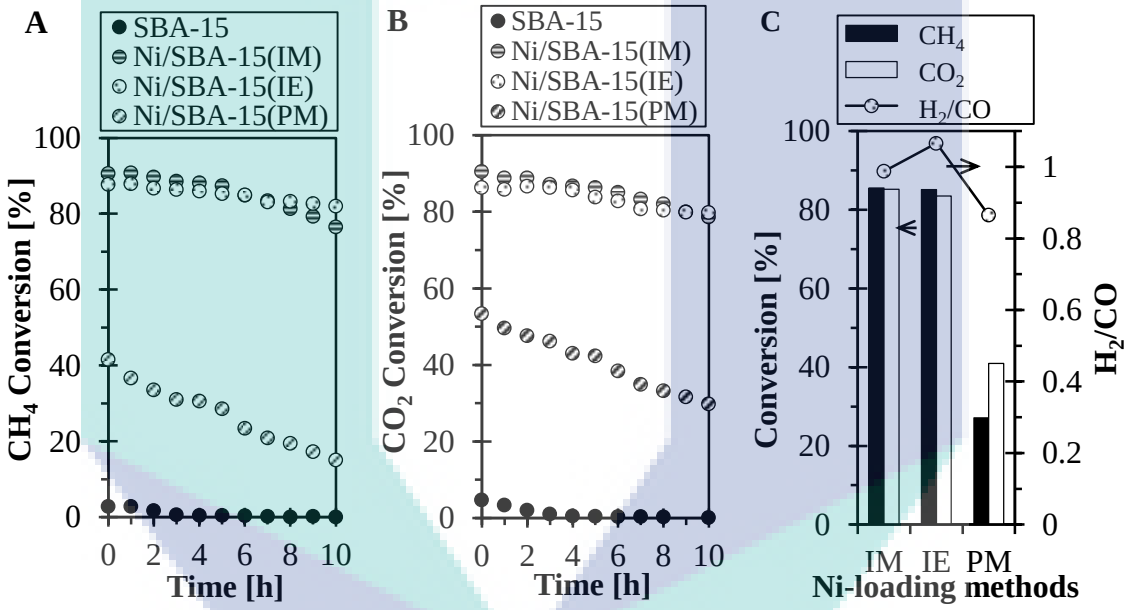

Figure 4.19: (A) CH_4 conversion and (B) CO_2 conversion of SBA-15, 3Ni/SBA-15, 5Ni/SBA-15 and 10Ni/SBA-15 in CO_2 reforming of CH_4. (C) Effect of Ni-loading methods on the CH_4 conversion, CO_2 conversion and H_2/CO ratio.

At temperature studied, the activity of catalysts followed the order of Ni/SBA-15(IE) ≈ Ni/SBA-15(IM) > Ni/SBA-15(PM), while the stability and H_2/CO ratio followed the order of Ni/SBA-15(IE) > Ni/SBA-15(IM) > Ni/SBA-15(PM). The lowest activity of Ni/SBA-15(PM) might be related to the larger Ni particles size arose from the weaker Ni-support interaction, where the Ni particles of PM method were preferentially agglomerate and decorating the surface part of SBA-15. Thus, it is believed that the Ni/SBA-15 that has higher Ni-support interaction are responsible for

the best catalytic performance with high stability, while, Ni/SBA-15 that has weaker Ni-support interaction results in the higher agglomeration of Ni particles and thus resulted in lower performance and stability.

The relationship between metal support interaction and catalytic activity of the catalyst was also observed on the Ni/MSN catalyst as reported by Sidik et al. (2016) (Sidik et al., 2016). They found that the Ni/MSN prepared by in-situ method has the highest catalytic activity as compared to impregnation and physical mixing methods due to the formation of strong metal support interaction (Si-O-Ni) through sequential desalination-substitution during the catalyst preparation. According to the proposed mechanism for CO_2 reforming of CH_4, the stepwise adsorption of CH_4 follows by its decomposition into CH_x fragments occurs on active metal sites, whereas CO_2 activation occurs mainly over the support. Thus, they claimed that the excellent catalytic activity is closely related to the availability of a great number of exposed Ni sites arose from the existence of strong metal support interaction (Si-O-Ni) which improved the dispersion of Ni active sites. In addition, Jing et al. (2004) studied the influence of metal support interaction on the catalytic performance of Ni/SrO-SiO_2. They found that the structure of the Ni active phase was strongly depended on the interaction between Ni and the support, which related to the preparation methods. Based on the results obtained, they claimed that the enhanced interaction between Ni species and SrO-SiO_2 might be responsible for the high activity of the catalyst towards the reformation of CH_4 with CO_2 and O_2. Therefore, on the basis of literature and the results obtained in this study, it is reasonable to conclude that the Ni-support interaction is responsible for an excellent catalytic performance and high stability of Ni/SBA-15 catalyst for CO_2 reforming of CH_4.

4.3.3 Summary on the Effect of Ni-Loading Methods on the Properties and Catalytic Activity of Ni/SBA-15 towards CO_2 Reforming of CH_4

In this study, a series of Ni/SBA-15 catalysts were prepared with three different methods which were impregnation (IM), ion exchange (IE) and physical mixing (PM). The results showed that the different Ni-loading methods influence the properties and catalytic performance of Ni/SBA-15 towards CO_2 reforming of CH_4. The characterization analyses showed that the quantity of metal support interaction followed

the order of Ni/SBA-15(IE) > Ni/SBA-15(IM) > Ni/SBA-15(PM), while the size of Ni particles, an agglomeration of Ni particles and blockage of the pores increased with the order of Ni/SBA-15(IE) < Ni/SBA-15(IM) < Ni/SBA-15(PM). At temperature studied, the activity of catalysts followed the order of Ni/SBA-15(IE) ≈ Ni/SBA-15(IM) > Ni/SBA-15(PM), while the stability of catalysts followed the order of Ni/SBA-15(IE) > Ni/SBA-15(IM) > Ni/SBA-15(PM). It was found that the introduction of Ni by IE resulted to the higher catalytic performance and stability, owing to the higher formation of Ni-support interaction by substitution of the Si-OH with Si-O-Ni. Meanwhile, the introduction of Ni by PM resulted to lower catalytic performance due to the higher agglomeration of Ni particles that were decorating on the surface part of SBA-15 arose from the weaker Ni-support interaction.

CHAPTER 5

CONCLUSION AND RECOMMENDATION

5.1 CONCLUSION

In this study, Ni/SBA-15 catalysts have been successfully prepared and characterized. The effects of TEOS/P123 mass ratios on the properties and catalytic activity of Ni/SBA-15 were studied by varying the TEOS/mass ratio (1.5, 2.21 and 3.0). Characterization results indicated that the TEOS/P123 ratio of 2.21 was the optimal synthesis ratio of Ni/SBA-15 which producing the well-ordered hexagonal mesoporous structure with the highest Ni-support interaction. The catalytic activity of Ni/SBA-15 towards CO_2 reforming of CH_4 followed the order of Ni/SBA-15(R2.21) > Ni/SBA-15(R3.0) > Ni/SBA-15(R1.5). The superior catalytic behavior of Ni/SBA-15(R2.21) towards CO_2 reforming of CH_4 was related with the catalytically favorable textural properties of Ni/SBA-15(R2.21) which enhanced the dispersion of metal particles, improved the catalyst activity, increased the catalyst stability and reduced the carbon deposition. Meanwhile, the lowest catalytic performance of Ni/SBA-15(R1.5) might be related with the incomplete hexagonal structure of SBA-15 which resulted in poorer dispersion of Ni particles as supported by the characterization results.

The effects of Ni content on the properties and catalytic activity of Ni/SBA-15 were studied by varying the amount of Ni content (3 – 10 wt%). XRD, BET and TGA results indicated that the increasing Ni loading (3–10 wt%) decreased the crystallinity, surface area and physically adsorbed water content of the catalysts. FTIR, TEM and H_2-TPR analysis confirmed the formation of Ni–O–Si by the substitution of surface silanol groups with Ni species and the maximum substitution of surface silanol groups with Ni were achieved at 5 wt%, while further increased in Ni loading stimulate the agglomeration of Ni particles. The activity of catalysts followed the order of 5Ni/SBA-

15 > 3Ni/SBA-15 ≈ 10Ni/SBA-15 > SBA-15. The superior catalytic performance of 5Ni/SBA-15 towards CO_2 reforming of CH_4 probably was related with the formation of metal-support interaction, Ni–O–Si, which enhanced the stabilization of the active Ni species on SBA-15 support and altered the properties of catalyst towards an excellent catalytic performance. The analysis of spent catalysts found that the presence of Ni–O–Si minimizes the growth of encapsulating graphite carbon and thus enhanced the stability of catalyst.

The effects of Ni-loading methods on the properties and catalytic activity of Ni/SBA-15 were studied by varying the preparation methods of Ni loading (impregnation (IM), ion exchange (IE) and physical mixing (PM)). The results showed that the different Ni-loading methods influence the properties and catalytic performance of Ni/SBA-15 towards CO_2 reforming of CH_4. The characterization analyses showed that the quantity of metal support interaction followed the order of Ni/SBA-15(IE) > Ni/SBA-15(IM) > Ni/SBA-15(PM), while the size of Ni particles, an agglomeration of Ni particles and blockage of the pores increased with the order of Ni/SBA-15(IE) < Ni/SBA-15(IM) < Ni/SBA-15(PM). At temperature studied, the activity of catalysts followed the order of Ni/SBA-15(IE) ≈ Ni/SBA-15(IM) > Ni/SBA-15(PM), while the stability of catalysts followed the order of Ni/SBA-15(IE) > Ni/SBA-15(IM) > Ni/SBA-15(PM). It was found that the introduction of Ni by IE resulted to the higher catalytic performance and stability, owing to the higher formation of Ni-support interaction by substitution of the Si-OH with Si-O-Ni. Meanwhile, the introduction of Ni by PM resulted to lower catalytic performance due to the higher agglomeration of Ni particles that were decorating on the surface part of SBA-15 arose from the weaker Ni-support interaction.

5.2 RECOMMENDATION FOR FUTURE WORK

As an extension of this study, further study can be done by using different types of methods for improving the dispersion of catalyst in order to reduce coke formation. In addition, the scale up of the laboratory reactor to a pilot plant size for this process also can be done in the future.

REFERENCES

Ababou, A., Ajbary, M., Taleb., M., & Kherbeche, A. (2015). CO_2 sequestration on new materials. *J. Mater. Environ. Sci*, *6*(9), 2367–2372.

Abderrahim, Berrebia, Hamou, Kherief, Zanoun, & Zenata. (2011). Measure of Carbon Dioxide using a Gas Sensor of a Semiconductor Type based on Tin Dioxide (SnO_2). *J. Mater. Environ. Sci*, *2*(1), 94–103.

Abdullah, A. Z., Razali, N., & Lee, K. (2010). Optimization of mesoporous K/SBA-15 catalyzed transesterification of palm oil using response surface methodology. *J. Phys. Sci.*, *21*(2), 13–27.

Ahmad, N. N. N., & Hossain, D. M. (2015). Climate Change and Global Warming Discourses and Disclosures in the Corporate Annual Reports: A Study on the Malaysian Companies. Procedia - Social and Behavioral Sciences. *Procedia-Social and Behavioral Science*, *172*, 246–253.

Aksoylu, A. E., Akin, A. N., Onsan, Z. I., & Trimm, D. L. (1996). Structure/activity relationships in coprecipitated nickel-alumina catalysts using CO_2 adsorption and methanation. *Appl. Surf. Sci*, *145*(1), 185–193.

Al-Fatesh, A. S. A., Fakeeha, A. H., & Abasaeed, A. E. (2011). Effects of Selected Promoters on Ni/γ-Al_2O_3 Catalyst Performance in Methane Dry Reforming. *J. Catal*, *32*(11), 1604–1609.

Albarazi, A., Gálvez, M. E., & Costa, P. D. (2015). Synthesis strategies of ceria–zirconia doped Ni/SBA-15 catalysts for methane dry reforming. *Catalysis Communication*, *59*, 108–112.

Alie, C., Backham, L., Croiset, E., & Douglas, P. L. (2005). Simulation of CO_2 capture using MEA scrubbing: a flowsheet decomposition method. *Energy Conversion and Management*, *46*, 475–487.

Allison, I., Colgan, W., King, M., & Paul, F. (2015). Ice Sheets, Glaciers, and Sea Level. Snow and Ice-Related Hazards. *Risk and Disaster*, *55*, 713–747.

Amin, M. H., Tardio, J., & Bhargava, S. K. (2012). A Comparison Study on Carbon Dioxide Reforming of Methane Over Ni Catalysts Supported on Mesoporous SBA-15, MCM-41, KIT-6 and g-Al2O3. *Material*, *270*, 136–145.

Aziz, M. A. A., Jalil, A. A., Triwahyono, S., & Saad, M. W. A. (2015). CO_2 reforming of methane over Ni supported on mesostructured silica nanoparticles (Ni/MSN): effect of Ni loading. *Chemical Engineering Journal*, *260*, 757–764.

Azlina, A. A., Law, S. H., & Mustapha, N. H. N. (2014). Dynamic linkages among transport energy consumption, income and CO_2 emission in Malaysia. *Energy Policy*, *73*, 598–606.

Bacariza, M. C., Graca, L., Aestermann, A., Ribeiro, M. F., Lopes, J. M., & Henriques, C. (2016). CO_2 Hydrogenation over Ni-Based Zeolites : Effect of Catalysts Preparation and Pre-reduction Conditions on Methanation Performance. *Topics in Catalyst*, 314–325.

Bao, X., Zhao, X. S., Li, X., & Li, J. (2004). A novel route toward the synthesis of high-quality large-pore periodic mesoporous organisilicas. *Appl. Surf. Sci*, *237*, 380–386.

Begum, R. A., Sohaga, K., Abdullah, S. M. S., & Jaafar, M. (2015). CO_2 emissions, energy consumption, economic and population growth in Malaysia. *Renewable and Sustainable Energy Reviews*, *41*, 594–601.

Benguerba, Y., Dehimi, L., Virginie, M., Dumas, C., & Ernst, B. (2015). Modelling of methane dry reforming over Ni/Al_2O_3 catalyst in a fixed-bed catalytic reactor. *Reaction Kinetic Mechanical Catalyst*, *114*(1), 109–119.

Berndt, F. M., & Perez-Lopez, O. W. (2016). Reaction kinetic mechanisms and catalysis impact factor. *Kinetic Mechanical Catalyst*, *4*(1), 1–13.

Bradford, M. C. J., & Vannice, M. A. (1997). Metal-support interactions during the CO2 reforming of CH4 over model TiO_x/Pt catalysts. *Catalytic Letter*, *48*, 31–38.

Brodie-Linder., N., Caër, S. Le, M., S. A., & Renault, J. P. (2010). H(2) formation by electron irradiation of SBA-15 materials and the effect of Cu(II) grafting. *Phy. Chem.*, *12*, 14188–14195.

Brodie-Linder, N., Caër, S. Le, Alam, M. S., Renault, J. P., & Alba-Simionesco, C. (2010). Physical Chemistry. *Phy. Chem.*, *12*, 14188–12195.

Cebrucean, D., Cebrucean, V., & Ionel, I. (2014). CO2 capture and storage from fossil fuel power plant. *Energy Procedia*, *63*, 18–26.

Chanadee, T., & Chaiyarat, S. (2016). Preparation and Characterization of Low Cost Silica Powder from Sweet Corn Cobs (Zea mays saccharata L.). *J. Mater. Environ. Sci*, *7*(7), 2369–2374.

Charan, P. H. K., & Rao, G. (2015). Synthesis and Catalytic Application of 12-Phosphotungstic Acid Encapsulated in SBA-15 by Impregnation and One-Pot Methods. *J. Chem. Sci.*, *127*, 909–919.

Crank, J., & Jacobe, P. (2015). Security Issues and Global Warming. *Crime, Violence and Global Warming*, *2*, 251–267.

Cui, Y., & Kump, L. R. (2015). Global warming and the end-Permian extinction event: Proxy and modeling perspectives. *Earth-Science Review*, *149*, 5–22.

Dan, M., Lazar, M. D., Mihet, M., Almasan, V., Rednic, V., & Borodi, G. (2012). Hydrogen production by low temperature methane steam reforming using Ag and Au modified alumina supported nickel catalysts. *Reaction Kinetic Mechanical Catalyst*, *105*(1), 173–193.

Devoy, R. J. N. (2015). Sea-Level Rise: Causes, Impacts, and Scenarios for Change. *Coastal and Marine Hazards, Risks, and Disasters*, *12*, 197–241.

Dijkstra, F. A., & Morgan, J. A. (2012). Elevated CO_2 and Warming Effects on Soil Carbon Sequestration and Greenhouse Gas Exchange in Agroecosystems: A Review. *Managing Agricultural Greenhouse Gases*, *121*, 467–486.

Donphai, W., Faungnawakij, K., Chareonpanich, M., & Limtrakul, J. (2014). Effect of Ni-CNTs/mesocellular silica composite catalysts on carbon dioxide reforming of methane. *Applied Catalysis A: General*, *121*, 467–486.

Fan, X. L., Zhao, J. Z., Wei, Y., Liu, J., Duan, A., & Jiang, G. (2015). Insights into the effects of steam on propane dehydrogenation over a Pt/Al_2O_3 catalyst. *Catal. Sci. Technology*, *5*(1), 339–350.

Fouad, O. A., Mohamed, R. M., M. S. Hassan, I., & Ibrahim, A. (2006). Synthesis and modification of ZSM-5 with manganese and lanthanum and their effects on decolorization of indigo carmine dye. *Catal. Today*, *116*, 82–87.

Guerrero, M. C. S., Lorenzo, E., M. F., Castillab, N., Sorianob, T., & Baillec, A. (2005). Effect of variable CO2 enrichment on greenhouse production in mild winter climates. *Agricultural and Forest Meteorology*, *132*, 244–252.

Habib, K., Schmidt, S., & Christen, J. H. (2013). A historical perspective of Global Warming Potential from Municipal Solid Waste Management. *Waste Management*, *33*, 1926–1935.

Haghighi, M., Sun, Z., Wu, J., Bromly, J., L., W. H., Ng, E., & Zhang, D. (2007). Catalysis science and Technology. *Proc. Combust Inst*, *31*(2), 1983–1990.

Harju, J., Sipila, O., & Juvela, M. (2015). On the stability of non-isothermal Bonnor-Ebert spheres. II. *The Effect of Gas Temperature on the Stability*, *582*, 48–52.

He, S. Y., He, S. H., Zhang, L., Li, X. F., Wang, J., He, D. D., & Luo, Y. M. (2015). Hydrogen production by ethanol steam reforming over Ni/SBA-15 mesoporous catalysts: Effect of Au addition. Catalysis. *Catal. Today*, *258*, 162–168.

Huang, Y. H., Chiueh, P. T., Shih, C. H., Lo, S. L., Sun, L. P., Zhong, Y., & Qiu, C. S. (2015). Microwave pyrolysis of rice straw to produce biochar as an adsorbent for CO2 capture. *Energy*, *84*, 75–82.

Isobe, M. (2013). Impact of global warming on coastal structures in shallow water. *Ocean Engineering*, *71*, 51–57.

Jennifer, M., Terry, L., & Stephen, J. T. (2013). A review of benefits and challenges in

growing street trees in paved urban environments. *Landscape and Urban Planning*, *222*, 493–501.

Jibran, M., Zuberia, & Alib, S. F. (2015). Greenhouse effect reduction by recovering energy from waste landfills in Pakistan. *Renewable and Sustainable Energy Reviews*, *44*, 117–131.

Jiménez, E., Fresno, T., Egea, C. L. De, & Peñalosa, J. M. (2010). Chemosphere Hydroponics as a valid tool to assess arsenic availability in mine soils. *Chemosphere*, *79*(5), 513–517.

Jing, Q., Lou, H., Fei J., H., Ou, Z., & Xi, Z. (2004). Syngas production from reforming of methane with CO_2 and O_2 over Ni/SrO-SiO_2 catalysts in a fluidized bed reactor. *International Journal of Hydrogen Energy*, *29*, 1245-1250.

Jung, J., Jeong, Y. S., Lim, Y. S., Lee, C. S., & Han, C. H. (2013). Advanced CO_2 capture process using MEA scrubbing: configuration of a split flow and phase separation heat exchanger. *Energy Proc*, *37*, 1778–1784.

Junke, X., Wei, Z., Jihui, W., Zhaojing, L., & Jianxin, M. (2009). Characterization and analysis of carbon deposited during the dry reforming of methane over Ni/La_2O_3/Al_2O_3 catalysts. *Chin J Catal*, *30*(11), 1076–1084.

Kajishima, T., Saito, T., Nagaosa, R., & Kosugi, S. (1997). GLAD: A gas-lift method for CO2 disposal into the ocean. *Energy*, *22*, 257–262.

Karclovic, A., & Ruiz, P. (2013). Mechanistic Study of Low Temperature CO_2 Metanation over RH/TiO_2 Catalysts. *J. Catal*, *301*, 141–153.

Karimi, M., Hillestad, M., & Svendsen, H. F. (2011). Capital costs and energy considerations of different alternative stripper configurations for post combustion CO_2 capture. *Chemical Engineering Research and Design*, *89*, 1229–1236.

Kaydouh, M. N., Hassan, N., Davidson, A., Casale, S., & Massiani, P. (2015). Highly active and stable Ni/SBA-15 catalysts prepared by a "two solvents" method for dry reforming of methane. *Microporous and Mesoporous Materials*, *220*, 99–109.

Keith, H., & Wong, H. C. (2006). Measurement of soil CO_2 efflux using soda lime absorption: both quantitative and reliable. *Soil Biology and Biochemistry*, *38*, 1121–1131.

Khajenoori, M., Rezaei, M., & Meshkani, F. (2015). Methane dry reforming over hydrotalcite-derived Ni–Mg–Al mixed oxides: the influence of Ni content on catalytic activity, selectivity and stability. *J. Ind. Eng. Chem*, *21*, 717–727.

Kordulis, C., Latsios, H., Lycourghiotis, A., & Pomonis, P. (2015). Kinetics of N_2O Decomposition on Fe^{3+}- Supported on Pure and Li-Modified Al_2O_3. *Int. J. Chem. Tech. Res.*, *88*, 201–205.

Kowalski, J., Linder, P., Zierke, S., Wulfen, B. V., Clemens, J., Konstantinidis, & K.,

Ameres, G. (2015). Navigation Technology for Exploration of Glacier Ice With Maneuverable Melting Probes. *Cold Regions Science and Technology*, *1*, 28–33.

Kruger, T. (2010). Enhanced weathering techniques: oceans. *Chemical Engineering*, *26*, 40–45.

Kruk, M., Jaroniec, M., Joo, S. H., & Ryoo, R. (2003). Characterization of the porous structure of SBA-15. *J. Phys. Chem. B*, *107*, 2205–2213.

Lang, A., Peter, J., & Kornmann, B. (2015). ER-mitochondria contact sites in yeast: beyond the myths of ERMES. *Curr Opin Cell Biol*, *35*, 7–12.

Lee, S. Y., & Holder, G. D. (2001). Methane hydrates potential as a future energy source. *Fuel Processing Technology*, *71*, 181–186.

Lee, Z. H., Sethupathi, S., Lee, K. T., Bhatia, B., & R, M. A. (2013). An overview on global warming in Southeast Asia: CO2 emission status, efforts done, and barriers. *Renewable and Sustainable Energy Reviews*, *28*, 71–81.

Li, L., Zhang, L. M., Zhang, Y. H., & Li, J. L. (2015). Effect of Ni loadings on the catalytic properties of Ni/MgO(111) catalyst for the reforming of methane with carbon dioxide. *Journal of Fuel Chemistry and Technology*, *43*, 315–322.

Liu, D., Quek, X.-Y., H.H.A. Wah, Zeng., G., Li, Y., & Yang, Y. (2009). MCM-41 supported nickel-based bimetallic catalysts with superior stability during carbon dioxide reforming of methane: Effect of strong metal–support interaction. *Catal. Today*, *148*, 243–250.

Liu, H., Li, Y., Wu, H., Liu, J., & He, D. (2014). Phycicoccus endophyticus sp. nov., anendophytic actinobacterium isolated from Bruguiera gymnorhiza. *Chin J Ctal*, *36*, 283.

Liu, J., Cui, D. M., Yu, J., Su, F. B., & Xu, G. W. (2015). CO methanation over a macro–mesoporous Al2O3 supported Ni catalyst in a fluidized bed reactor. *Chin J Chem. Eng*, *23*(1), 86–92.

Liu, Q., Dong, X., & Z. Liu. (2014). Material Chemistry. *Chin J Chem. Eng*, *22*(2), 131–135.

Lovell, B. (2015). Paleogene silcretes and the 55 Ma global warming event: is there proof in the Hertfordshire Puddingstone. *Proceedings of the Geologists' Association*, *23*, 57–88.

Lu, B., & Kawamoto, K. (2014). NiO/SBA15. *Inter. Coal Sci. Technol*, *1*(2), 315–320.

Lunde, P. J., Frank, L., & Kester. (1974). Carbon Dioxide Methanation on a Ruthenium Catalyst. *Ind. Eng. Chem. Process*, *13*(1), 27–33.

Machlin, E. ., & Weining, S. (1953). Le Chatelier's principle and stress-induced displacive transformations. *Acta Metallurgica*, *1*(5), 480–482.

Martínez, A., López, C., Márquez, F., & Díaz, I. (2003). Synthesis of Hydrocarbons over mesoporous Co/SBA-15 Catalysts: The influence of metal loading, cobalt precursor and promoter. *Journal of Catalysis*, *220*, 486–499.

McGlashan, N., Shah, N., C., Aldecott, B., & Workman, M. (2012). High-level techno-economic assessment of negative emissions technologies. *Process Safety and Environmental Protection*, *90*, 501–510.

Moioli, S., Pellegrini, L. A., & Gamba, S. (2012). Simulation of CO_2 capture by MEA scrubbing with a rate based model. *Procedia Engineering*, *42*, 1651–1661.

Molloy, S. L., & Mihaltcheva, S. (2013). Greenhouse effect, sea level rise and land use. *Land Use Policy*, *7*, 138–153.

Mugable, M. I. (2013). Analysing the CO_2 Emissions Function in Malaysia: Autoregressive Distributed Lag Approach. *Procedia Economics and Finance*, *5*, 571–580.

Mustapa, S. I., & Bekhet, H. A. (2015). Investigating Factors Affecting CO_2 Emissions in Malaysian Road Transport Sector. *International Journal of Energy Economics and Policy*, *5*(4), 1073–1083.

Mutz, B., Hudson, W. P., Carvalho, Mangold, S., Kleist, W., & Grunwaldt, J. D. (2015). Methanation of CO_2: Structural response of a Ni-based catalyst under fluctuating reaction conditions unraveled by operando spectroscopy. *Journal of Catalysis*, *327*, 48–53.

Natesakhawat, S., Reza, B. W., Xi, Q. W., & Una, S. O. (2005). Deactivation characteristics of lanthanide-promoted sol–gel Ni/Al2O3 catalysts in propane steam reforming. *J Catal*, *2*, 496-500.

Nematollahi., B., Rezaei, M., & Khajenoori, M. (2011). Combined Dry Reforming and Partial Oxidation of Methane to Synthesis Gas on Noble Metal Catalysts. *Int. J. Hydrogen Energy*, *36*, 2969–2978.

Nielsen, I., Nielsen, O., Muray, J., & Thon, G. (2002). The fission yeast ubiquitin-conjugating enzymes UbcP3, Ubc15, and Rhp6 affect transcriptional silencing of the mating-type region. *Eukaryot Cell*, *1*(4), 613–25.

Oemar, U., Kathiraser, Y., Mo, L., Ho, X. K., & Kawi, S. (2016). CO_2 reforming of methane over highly active La-promoted Ni supported on SBA-15 catalysts: mechanism and kinetic modelling. *Catal. Sci. Technology*, *6*, 1173–1186.

Park, K., Moon, S., Kim, S., & Jeon, S. (2009). Ectopic Repo suppresses expression of castor gene in Drosophila central nervous system. *Biochem. Biophys Res Commun*, *388*(2), 187–192.

Qi, Y., Cheng, Z., & Zhou, Z. (2015). DNA sequence alignment by microhomology sampling during homologous recombination. *J. Chem. Eng.*, *23*, 76–85.

Qian, Y., Kachroo, A., Yellman, C. M., & Johnson, K. (2014). Yeast Cells Expressing the Human Mitochondrial DNA Polymerase Reveal Correlations between Polymerase Fidelity and Human Disease Progression. *J Biol Chem*, *289*(9), 5970–85.

Rahemi, N., Haghighi, M., Babaluo, A. K., Allahyari, S., & Jafari, M. (2014). CO_2 reforming of methane over Ni-Cu/Al_2O_3-ZrO_2 nanocatalyst : The influence of plasma treatment and process conditions on catalytic properties and performance. *Optik - International Journal for Light and Electron Optics*, *84*, 50–59.

Rebitanim, N. Z., Ghani, W. A. W. A. K., Rebitanim, N. A., & Salleh M. A. M. (2013). Potential applications of wastes from energy generation particularly biochar in Malaysia. *Renewable and Sustainable Energy Reviews*, *21*, 694–701.

Richardson, J. T., Garrait, M., & Hung, J.-K. (2003). Carbon Dioxide Reforming with Rh and Pt-Re Catalysts Dispersed on Ceramic Foam Supports. *Applied Catalysis A: General*, *255*(1), 69–82.

Roscher, M., Stordal, F., & Vensen, H. (2011). The effect of global warming and global cooling on the distribution of the latest Permian climate zones. *Palaeogeography, Palaeoclimatology, Palaeoecology*, *309*, 186–200.

Sajjadi, S. M., Haghighi, M., Eslami, A. A., & Rahmani, F. (2013). Hydrogen production via CO_2-reforming of methane over Cu and Co doped Ni/Al_2O_3 nanocatalyst: impregnation versus sol–gel method and effect of process conditions and promoter. *J. Sol-Gel Sci. Tech*, *67*, 601–617.

Setiabudi, H. D., A.A., T. J., & Riwahyono, S. (2012). Ir/Pt-HZSM5 for n-pentane isomerization: Effect of iridium loading on the properties and catalytic activity. *Journal of Catalyst*, *294*, 128–135.

Setiabudi, H. D., Razak, N. S. A., Suhaimi, F. R. M., & Pauzi, F. N. (2016). CO_2 reforming of CH4 over Ni/SBA-15: Influence of Ni-loading methods. *Malaysian Journal of Catalyst*, *1*, 1–6.

Setiabudi, H. D., Triwahyono, S., Jalil, A. A., Kamarudin, N. H. N., & Aziz, M. A. . (2011). Effect of iridium loading on HZSM-5 for isomerization of n-heptane. *J. Nat. Gas. Chem*, *20*, 477–480.

Sidik, S. M., Triwahyono, S., Jalil, A. A., Aziz, M. A. A., & Fatah, N. A. (2016). Tailoring the properties of electrolyzed Ni/mesostructured silica nanoparticles (MSN) via different Ni-loading methods for CO_2 reforming of CH_4. *Journal of CO_2 Utilization*, *13*, 71–80.

Sina, N., Nasiri, S., & Karkhaneh, V. (2015). Effects of resistive loads and tire inflation pressure on tire power losses and CO2 emissions in real-world condition. *Applied Energy*, *157*, 974–983.

Singh, D., Croiset, E., Douglas, P. L., & Douglas, M. A. (2003). Techno-economic study of CO_2 capture from an existing coal-fired power plant: MEA scrubbing vs. O_2/CO_2 recycle combustion. *Energy Conversion and Management*, *44*, 3073–3091.

Solymosi, F., Erdöhelyi, A., & Bánsági, T. (1981). Methanation of CO_2 on suppoted rhodium catalyst. *Journal of Catalysis*, *68*, 371–382.

Son, I. H., Lee, S. J., Song, I. Y., Jeon, W. S., Jung I., Y., Un, D. J., & Roh, H.-S. (2014). Industrial Catalytic Processes for Fine and Specialty Chemicals. *Fuel*, *36*, 194–200.

Tan, J., C., Jakob, W. B., & Rossow, G. (2015). Increases in tropical rainfall driven by changes in frequency of organized deep convection. *Nature*, *519*, 451–454.

Tao, K., Zhang, Y., Terao, S., & Tsubaki, N. (2010). Development of platinum-based Bimodal pore catalyst for CO2 reforming of CH4. *Chemical Engineering*, *153*, 150–155.

Theofanidis, S. A., Galvita, V. V., Poelman, H., & Marin, G. B. (2015). Enhanced Carbon-Resistant Dry Reforming Fe-Ni Catalyst: Role of Fe. *ACS Catalyst*, *5*, 3028–3039.

Thoma, M., Determann, J., Grosfeld, K., Goeller, S., & Hellmer, H. H. (2015). Future sea-level rise due to projected ocean warming beneath the Filchner Ronne Ice Shelf: A coupled model study. *Earth and Planetary Science Letters*, *431*, 217–224.

Thomazini, A., Spokas, K., Hall, K., Ippolito, J., Lentz, R., & Novak, J. (2015). GHG impacts of biochar: Predictability for the same biochar. *Agriculture, Ecosystems & Environment*, *207*, 183–191.

Vafaeian, Y., Haghighi, M., & Aghamohammadi, S. (2013). Ultrasound Assisted Dispersion of Different Amount of Ni over ZSM-5 Used as Nanostructured Catalyst for Hydrogen Production via CO_2 Reforming of Methane. *Energy Convers. Manag*, *76*, 1093–1103.

Valle, M., Chust, G., Campo, A. D., Wisz, M. S., Olsen, S. M., Garmendia, J. M., & Borja, A. (2014). Projecting future distribution of the seagrass Zostera noltiiunder global warming and sea level rise. *Biological Conservation*, *170*, 74–85.

Wang, C. H., Guo, D. F., Li, Z. F., Wang, X. M., Lin, J. H., Zeng, Z. Z., & Jing, X. P. (2012). Crystal structure of $Sr_6Y_2Al_4O_{15}$: XRD refinements and first-principle calculations. *Journal of Solid State Chemistry*, *192*, 195–200.

Wang, H., Zhang, Y., Guo, Y., Zhang, L., Han, Y., & Zhao, X. (2016). Visible-light-driven oxidation of cyclohexane using Cr-supported mesoporous catalysts prepared via phenyl-functionalized mesoporous silica. *RSC Advance*, *6*(44), 38176–38182.

Wang, N., Yu, X., Wang, Y., Chu, W., & Lu, M. (2013). CO_2 Reforming of CH_4 over MgO-Doped Ni/MAS-24 with Microporous ZSM-5 Structure. *Catal. Today*, *212*,

98–107.

Wu, C. F., Budarin, V. L., Wang, M. H., Sharifi, V., Gronnow, M. J., & Wu, Y. J. (2015). CO_2 gasification of bio-char derived from conventional and microwave pyrolysis. *Applied Energy*, *157*, 533–539.

Xia, F., Ou, E., Wang, L., & Wang, J. (2008). Photocatalytic degradation of dyes over cobalt doped mesoporous SBA-15 under sunlight. *Dye Pigmen*, *76*, 76.

Xu, J., Lin, Q., Su, X., Duan, H., H., H. G., & Uang, Y. (2016). Nanostructured energy materials for electrochemical energy conversion and storage: A review. *Chin J Chem. Eng*, *24*, 140–145.

Ye, W., Lin, Z., Dong, B., Kang, J., Zheng, X., & Wang, X. (2011). Preparation and Catalytic Properties of Ti-SBA-15 Mesoporous Materials. *Material Science and Application*, *2*, 661–668.

Zamani, A., Mirshamsi, O., & Marusik, Y. (2014). The checklist of spider of Iran. *Arachnologis Mitteihunger*, *41*, 41–44.

Zhang, J. S., & Li, F. . (2015). Coke resistant Ni/SiO_2 catalyst for dry reforming of methane. *Applied Catalysis B: Environmental*, *176*, 513–521.

Zhang, X., Zhang, S. H., Yang, H. P., Feng, Y., Chen, Y. Q., Wang, X. H., & Chen, H. P. (2014). Nitrogen enriched biochar modified by high temperature CO_2–ammonia treatment: Characterization and adsorption of CO_2. *Chemical Engineering Journal*, *257*, 20–27.

Zhao, D., Feng, J., Huo, Q., Melosh, N., Fredrickson, G. H., Chmelka, B. F., & Stucky, G. D. (1998). Triblock Copolymer Syntheses of Mesoporous Silica with Periodic 50 to 300 Angstrom Pores. *Science*, *279*, 548–552.

APPENDIX A

RESEARCH OUTPUTS

List of Publication

1. H.D. Setiabudi, N.S.A. Razak, F.R.M. Suhaimi, F.N. Pauzi, CO_2 reforming of CH_4 over Ni/SBA-15: Influence of Ni-loading methods, Malaysian Journal of Catalysis 1 (2016) 1-6. (eISSN:0128-2581, Non-index Journal)
2. H.D. Setiabudi, K.H. Lim, N. Ainirazali, S.Y. Chin, N.H.N. Kamarudin, CO_2 reforming of CH_4 over Ni/SBA-15: Influence of Ni loading on the metal-support interaction and catalytic activity, Journal of Materials and Environmental Sciences 8(2) (2017) 573-581. (ISSN: 2028-2508, Index Journal, JIF: 1.21)
3. C.Y. Chin, S.N. Bukhari, H.D. Setiabudi, N. Ainirazali, Dai-Viet N. Vo, CO_2 reforming of CH_4 over Ni/SBA-15: Influence of TEOS/P123 mass ratio on the properties and catalytic activity, Submitted to Journal of Energy Chemistry. (ISSN:2095-4956, Index Journal, Thomson Reuters Impact Factor: 2.322)

List of Conferences

1. H.D. Setiabudi, N. Ainirazali, S.F.R.M. Suhaimi, F.N. Pauzi, K.H. Lim, S.Y. Chin, CO_2 reforming of CH_4 over Ni/SBA-15 catalyst: Effect of Nickel loading, 4th Conference on Emerging and Process Technology 2015, 15-16 December 2015, Melaka.
2. H.D. Setiabudi, S.M. Abed, N. Ainirazali and S.Y. Chin, CO_2 reforming of CH_4 over Ni-Ce/SBA-15: Effect of Ni-Ce loading methods, International Conference on Catalysis 2016, 20-21 September 2016, Johor.

Exhibitions

1. Chin Chia Yun, Herma Dina Setiabudi, Design and development of Ni/SBA-15 for CO_2 reforming of CH_4, 2016 Creation, Innovation, Technology & Research

Exposition (CITREX 2016), 7-8 March 2016, Universiti Malaysia Pahang, Pahang. (Bronze)

2. Lim Kiang Hoo, Herma Dina Setiabudi, Nurul Aini Mohamed Razali, Development of Ni/SBA-15 catalyst and its potential in enhancing syngas production, 2016 Creation, Innovation, Technology & Research Exposition (CITREX 2016), 7-8 March 2016, Universiti Malaysia Pahang, Pahang. (Bronze)
3. Siti Nuraihan Mohd Arof, Nurul Aini Mohamed Razali, Herma Dina Setiabudi, Production of Hydrogen over Ni/SBA-15 catalyst, 2016 Creation, Innovation, Technology & Research Exposition (CITREX 2016), 7-8 March 2016, Universiti Malaysia Pahang, Pahang. (Bronze)

List of Students

Master Research Project

1. Saad Mohsin Abed (KKK14005), Production of Syngas from CO_2 Reforming of CH_4 using Ni-Ce/SBA-15 Catalyst, Master Research Project, 2016.
2. Abderahman Hamad Khalifa Owgi (KKE16007), Synthesis and Characterization of Surfactant-Assisted Ni/SBA-15 Catalysts for CO_2 Dry Reforming of CH_4, Master Research Project, 2016.

Undergraduate Research Project

1. Chin Chia Yun (KA12108), Carbon Dioxide Reforming of Methane over Ni-promoted SBA-15: Effect of TEOS/P123 Mass Ratio, Undergraduate Research Project, 2016.
2. Lim Kiang Hoo (KA12105), CO_2 Reforming over Nickel/SBA-15 Catalyst: Effect of Nickel Loading, Undergraduate Research Project, 2016.
3. Noor Syahira bt Abd Razak (KA12057), CO_2 Reforming Methane over Nickel/SBA-15 Catalyst: Effect of the Preparation Method, Undergraduate Research Project, 2016.